



TALLINN UNIVERSITY OF TECHNOLOGY
SCHOOL OF ENGINEERING
Department of Materials and Environmental Technology

**SYNTHESIS OF PLATINUM-MODIFIED
NANOCARBON CATALYSTS FOR FUEL CELL
APPLICATION**

**PLAATINAGA MODIFITSEERITUD SÜSINIK-
NANOMATERJALID KÜTUSEELEMENTIDE TARVIS**

MASTER THESIS

Student: Erkin NAJAFI
Student code: 184645KAYM
Supervisor: Dr. Ivar KRUUSENBERG, Senior Research Fellow

Tallinn 2020

(On the reverse side of title page)

AUTHOR'S DECLARATION

Hereby I declare, that I have written this thesis independently.

No academic degree has been applied for based on this material. All works, major viewpoints, and data of the other authors used in this thesis have been referenced.

"....." 20.....

Author:

/signature /

Thesis is in accordance with terms and requirements

"....." 20....

Supervisor:

/signature/

Accepted for defence

"....."20... .

Chairman of theses defence commission:

/name and signature/

Department of Materials and Environmental Technology

THESIS TASK

Student: Erkin Najafli, 184645KAYM

Study programme: KAYM, Materials and Processes for Sustainable Energetics

Main speciality: Processes for Sustainable Energetics

Supervisor: Senior Research Fellow, Ivar Kruusenberg, +3725036963

Thesis topic:

SYNTHESIS OF PLATINUM-MODIFIED NANOCARBON CATALYSTS FOR FUEL CELL APPLICATION (in English)

PLAATINAGA MODIFITSEERITUD SÜSINIK-NANOMATERJALID KÜTUSEELEMENTIDE TARVIS (in Estonian)

Thesis main objectives:

1. Determining the influence of different pre-treatment methods on final catalyst properties
2. Comparison of synthesized samples among each other and to the commercial Pt catalyst
3. Conducting detailed analysis of electrochemical, SEM, EDX, XRD and Raman characterizations

Thesis tasks and time schedule:

No	Task description	Deadline
1.	Synthesizing total of four pre-treated and non-treated catalysts	14.02.2020
2.	Analyzing the characterization results and drawing conclusions	17.03.2020
3.	Writing the thesis	22.05.2020

Language: English

Deadline for submission of thesis: 26 May 2020

Student: Erkin Najafli "....."201....a
/signature/

Supervisor: Dr. Ivar Kruusenberg "....."201....a
/signature/

Head of study programme: Prof. Sergei Bereznev "....."201....a
/signature/

Terms of thesis closed defence and/or restricted access conditions to be formulated on the reverse side

Inseneriteaduskond

AVALDUS

Palun piirata ligipääs minu magistritööle teemal „Synthesis Of Platinum-Modified Nanocarbon Catalysts For Fuel Cell Application/Platinaga Modifitseeritud Süsinik-Nanomaterjalid Kütuseelementide Tarvis“ ja mitte avalikustada seda TalTech digikogus kuna töö sisaldab veel avaldamata materjale. Materjalid avalikustatakse, 20.05.2022 peale mida võib töö avalikustada.

Lugupidamisega

allkiri

Erkin Najafli

21.05.2020

Kooskõlastatud:

Ivar Kruusenberg, Ph.D.

Kooskõlastatud:

Dekaan/ prodekaan

Kooskõlastatud:

Kaitsmiskomisjoni esimees

CONTENTS

List of abbreviations and symbols.....	7
INTRODUCTION	8
1. LITERATURE REVIEW AND STUDY OBJECTIVES	10
1.1 A brief history of fuel cell technology.....	10
1.2 Fuel cell types and the working principle.....	11
1.2.1 Proton-exchange membrane fuel cell (PEMFC)	11
1.2.2 Alkaline fuel cell (AFC).....	13
1.2.3 Phosphoric acid fuel cell (PAFC).....	14
1.2.4 Molten carbonate fuel cell (MCFC).....	14
1.2.5 Solid oxide fuel cells (SOFC)	15
1.3 Oxygen reduction reaction.....	16
1.3.1 Kinetics of ORR.....	16
1.3.2 Pt-based catalyst materials used in the ORR.....	17
1.3.3 Alternatives to the Pt-based catalyst materials.....	19
1.3.4 Pre-treatment of carbon black.....	20
1.4 Pt/C synthesis methods	20
1.4.1 Comparison of various chemical synthesis methods.....	21
1.5 Summary of the literature review and aim of the study	23
2. EXPERIMENTAL.....	25
2.1 Pre-treatment of carbon black.....	25
2.2 Synthesis of the catalyst	26
2.2.1 Pt/XC polyol synthesis protocol	26
2.2.2 Pt/N-doped XC polyol synthesis protocol	26
2.3 Characterization techniques and equipment	27
2.3.1 Electrochemical characterization.....	27
2.3.2 X-ray diffraction (XRD)	29
2.3.3 Scanning electron microscopy (SEM).....	30
2.3.4 Raman spectroscopy	30
3. RESULTS AND DISCUSSION.....	31
3.1 RDE results.....	31
3.1.1 Electrochemically active surface area (EASA) determination..	31
3.1.2 ORR activity	32
3.1.3 Influence of pre-treatment on the catalytic activity of Pt/XC-72R (H ₂ O ₂ treated)	34
3.1.4 Koutecky-Levich analysis	35
3.1.5 Accelerated stress testing (AST) result	38
3.2 SEM images and EDX spectra.....	39
3.3 XRD results.....	41
3.4 Raman spectra	42
4. CONCLUSIONS	45
REFERENCES.....	47

PREFACE

This thesis topic was suggested by Dr. Ivar Kruusenberg, a senior research fellow at NICPB (National Institute Of Chemical Physics And Biophysics). The major part of the work was performed at the Laboratory of Energy Technologies in NICPB. For the experimental and data interpretation parts, I consulted fellow researchers (Ehsan Zarmehri, Kätlin Kaare, Dr. Kerli Liivand, Maryam Kazemi, and Sander Ratso) at the laboratory. I was also assisted by Dr. Maarja Grossberg, Dr. Peter Walke, and Dr. Valdek Mikli from Tallinn University of Technology. In general, the thesis was supervised by Dr. Ivar Kruusenberg.

I would like to thank my supervisor for introducing me to his project where I gained hands-on research experience and motivation for further academic study. At the same time, I am grateful to all individuals who did not hesitate to share their precious knowledge with me and provided guidance at tough times. Last but not least, I wish to show my appreciation for the endless support, inspiration, and encouragement I received from my dear family and friends.

The work was financed by Estonian Research Council's Personal Start-up Grant (PSG 312) and ERA.Net RUS Plus grant "HeDoCat".

The main focus of this research was studying the effect of carbon support chemical pre-treatment on the final catalyst properties for the oxygen reduction reaction in a fuel cell. The aim was to achieve improved activity while not changing the amount of platinum used in the catalyst which can play a vital role to cut overall fuel cell stack cost and facilitate the commercialization process. For this purpose, two different pre-treatment methods were employed and in total four catalysts were synthesized via polyol technique. After conducting several characterization studies and measurements, it was concluded that hydrogen peroxide treatment of vulcan carbon enhances the catalytic activity while nitric acid treatment was not associated with the desired improvement in catalyst properties.

Keywords: Fuel cell, platinum catalyst synthesis, vulcan carbon, chemical pre-treatment, oxygen reduction reaction, master thesis.

List of abbreviations and symbols

AEM – Anion exchange membrane	MA – Mass activity
AEMFC – Anion exchange membrane fuel cell	MCFC – Molten carbonate fuel cell
AFC – Alkaline fuel cell	n – Number of electrons
AST – Accelerated stress testing	η – Overpotential
Atom. C – Atomic concentration	η_{conc} – Concentration overpotential
B – Levich constant	N-doped – Nitrogen doped
BSE – Backscattered electrons	η_{act} – Activation overpotential
C – Carbon black	Norm. C – Normalised concentration
C_0 – Bulk concentration of oxygen	NP – Nanoparticle
CV – Cyclic voltammetry	ORR – Oxygen reduction reaction
DCDA – Dicyandiamide	PAFC – Phosphoric acid fuel cell
D_0 – Diffusion coefficient for oxygen	PEM – Proton-exchange membrane
ΔE – Potential	PEMFC – Proton-exchange membrane fuel cell
E^0 – Standard electrode potential	PGM – Platinum group metals
E_{eq} – Equilibrium potential	pH – Power of hydrogen
E_{onset} – Onset potential	Pt/C – Platinum on carbon black support
E_r – Resultant potential	PTFE membrane – Polytetrafluoroethylene
EASA – Electrochemically active surface area	PVP – Polyvinylpyrrolidone
EDX – Energy dispersive X-ray spectroscopy	$Q_{\text{h.des}}$ – Charge of H desorption region
EG – Ethylene glycol	Q_{ref} – Charge required for monolayer adsorption of hydrogen on Pt surface
F – Faraday constant	RDE – Rotating disk electrode
FC – Fuel cell	RHE – Reversible hydrogen electrode
FCC – Face-centered cubic	RPM- Revolutions per minute
FCV – Fuel cell vehicle	SA – Specific activity
Fe-N-C – Nitrogen-coordinated iron on carbon	SCE – Saturated calomel electrode
FEG – Field emission gun	SE – Secondary electrons
HOR – Hydrogen oxidation reaction	SEM – Scanning electron microscopy
I_D – D-band intensity	SOFC – Solid oxide fuel cell
I_G – G-band intensity	SHE – Standard hydrogen electrode
iR – Ohmic drop	Unn. C – Unnormalised concentration
j – Current density	ν – Kinematic viscosity
j_k – Kinetic-limited current density	ω – Angular velocity
j_{lim} or j_l – Diffusion-limited current density	XC – Vulcan XC-72R (type of carbon black)
k – Electron transfer rate constant	XRD – X-ray diffraction
KL – Koutecky-Levich	YSZ – Yttria-stabilized zirconia
LSV – Linear sweep voltammogram	

INTRODUCTION

With the rising concerns regarding the traditional fossil fuel-based energy production, transmission, and utilization cycle, countermeasures led by the clean energy technologies are causing a paradigm shift. Among the emerging electrical energy production technologies, the fuel cell is one of the devices that holds a promising potential for an efficient transition to the carbon-free future. The main property to define a type of fuel cell is the kind of electrolyte used in the system. For instance, alkaline fuel cells employ aqueous alkaline solution as the electrolyte and thus they are called so. The common type of fuel used in the fuel cells is hydrogen. In simple terms, the hydrogen fuel cell generates electricity from electrons flow while recombining hydrogen and oxygen back to the water form.

There are several pros and cons associated with hydrogen fuel cell technology. For instance, as the technology can also be embedded in the renewable energy systems, it may be used as a means to convert the hydrogen stored during the excess energy production of a solar panel and thus make the whole process more energy and cost-efficient. Apart from this, the fuel cells have a competitive edge over similar devices with their high electrical conversion efficiency, significantly less environmental pollution, higher energy density figures, etc. They are also practical to use for long-term performance as the fuel cell operates as long as there is a fuel intake provided. However, drawbacks like a strong need for complete hydrogen infrastructure, high cost of certain materials used in the cell, and other specific issues (for example operating in high temperature) are yet to be solved.

One of the key aspects to overcome the drawbacks is reducing the amount of platinum-group metals (PGM) used in the fuel cell's electrodes as an electrocatalyst. In an electrochemical reaction, electrocatalyst speeds up the rate of the reaction while not being affected in the process. Owing to the sluggish kinetics of hydrogen oxidation reaction (HOR) at the anode and oxygen reduction reaction (ORR) at the cathode of the hydrogen fuel cell, platinum-based electrocatalysts are often used to increase the speed of the reactions. As the platinum catalysts constitute around 40% of the fuel cell stack cost (see Fig. 1.1.), by reducing the amount of platinum used in the stack, the cost of the technology can be considerably cut down and thus affordable market value would be obtained. This can also be attained by boosting the catalytic activity without increasing the amount of Pt used in the system. One of the suggested ways to do so is pre-treatment of the catalyst's support material to increase its activity towards ORR.

In this work, four types of Pt-based catalyst materials were synthesized and evaluated based on several measurements. The aim of the study was to research the influence of support pre-treatment on the final characteristics of the catalyst. By comparing catalysts prepared by different treatment techniques among themselves and to other samples such as non-treated carbon, commercial and N-doped catalysts, it is possible to determine a procedure that can help with achieving enhanced properties without changing the Pt loading.

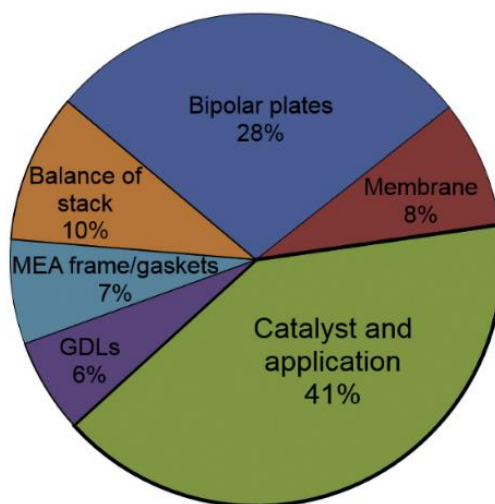


Fig. 1.1. Component cost breakdown at a production volume of 500,000 units/year for the FC stack [1]

After the synthesis, all of the samples were characterized by using various electrochemical and physical characterization methods. To carry out the electrochemical measurements, a conventional three-electrode system was used to acquire cyclic voltammetry curves. For later part of the study, the effect of pre-treatment was mainly examined in case of the catalyst prepared by using the H_2O_2 pre-treatment due to superior results obtained for this sample. The surface morphology of the resulting catalyst material was studied using SEM. Then, XRD and Raman spectra for each sample were collected in order to specify the microstructure of both Pt and C present in the materials.

The thesis consists of three main chapters. In the first part of the study, a literature overview has been carried out to discuss the general principles and history of fuel cells focusing principally on the catalyst materials used in these systems. For the second and experimental part, synthesis/pre-treatment methods and procedures employed in this work were written in detail. Finally, the latter chapter was devoted to obtained results and it provides detailed discussion with final remarks. References can be found in the end after the discussion part.

1. LITERATURE REVIEW AND STUDY OBJECTIVES

1.1 A brief history of fuel cell technology

The first raw form of fuel cell device is considered to be designed by the British scientist Sir Humphry Davy in the early 19th century [2]. His design was a simple form of an electrochemical cell with carbon anode and nitric acid electrolyte that could produce electricity with the help of the electrolysis (splitting water into hydrogen and oxygen by applying electrical current) process. However, a more sophisticated type of fuel cell device that fits the modern description was created independently by Christian Schönbein (German scientist) and William Grove (British scientist). The scientists were investigating the concept of reversing the electrolysis and using H₂ and O₂ to produce electricity. *The London and Edinburgh Philosophical Magazine and Journal of Science* published Grove's letter in 1838, while Schönbein's letter was published in 1839 making William Grove to be regarded as the inventor.

In fact, the modern phosphoric acid fuel cell is a derivative of the first fuel cell designed by Grove [3]. The so-called "Grove cell" had sulphuric acid as the electrolyte with two electrodes to which H₂ and O₂ were provided. Nevertheless, Charles Langer and Ludwig Mond were the first to coin the word "fuel cell" in 1889 while developing a cell working with coal gas and oxygen which was later not completed due to the emerging internal combustion engine technology. Next, proton exchange membrane fuel cell was developed by two General Electric scientists Thomas Grubb and Leonard Niedrach in 1955 which was used in NASA's Gemini space program flights to produce electricity. About 4 years later, British scientist Francis Bacon who was studying the alkaline fuel cell systems since the 1930s revealed the "Bacon cell" with 5 kW power output. Around the same time, NASA adopted the alkaline fuel cells for the Apollo space mission.

The research to identify alternative means to generate power was initiated around the 1970s after the oil crisis and this resulted in the development of further fuel cell technologies such as the modern phosphoric acid, solid oxide, and molten carbonate fuel cells. However, the high cost of these technologies was a major restriction against their commercialization. The first commercial phosphoric acid fuel cell system was pioneered by the International Fuel Cells (Toshiba and UTC's subsidiary) in the 1990s. Direct methanol fuel cell was the next type of fuel cell to be invented around the same time with its relatively low weight that allowed the cell to be portable. Since then, bottlenecks of the fuel cell technology are sought to be eliminated with the help of expanded research and introduction of the first commercial fuel cell vehicle of Toyota Mirai was a major milestone achieved in this quest [4].

1.2 Fuel cell types and the working principle

Apart from the type of electrolyte used in the system, it is possible to characterize fuel cell (FC) types based on their operating temperature. In case of the low-temperature FCs like Proton-Exchange Membrane Fuel Cells (PEMFC), Alkaline Fuel Cells (AFC), and Phosphoric Acid Fuel Cells (PAFC) the desired activity in the electrodes is reached with the help of using noble metals as electrocatalysts. In contrast, Molten Carbonate Fuel Cells (MCFC) and Solid Oxide Fuel Cells (SOFC) are high-temperature FCs that are not restricted to employ noble metal-based catalysts for speeding up the reaction [5]. The operating temperature is also critical for the type of fuel that can be fed into the FC. While hydrogen is the prevalent fuel type for the PEMFC, AFC, and PAFCs, CO can be used as an alternative fuel for high-temperature FCs as shown in Table 1.1.

Table 1.1. Materials used in the fuel cells [5]

Fuel cell type	Electrolyte	Cathode	Anode	Temperature	Fuel
SOFC	Y ₂ O ₃ - stabilized ZrO ₂ (YSZ)	Sr-doped LaMnO ₃	Ni/YSZ	800-1000 °C	H ₂ , CO
MCFC	Li ₂ CO ₃ , K ₂ CO ₃	Li-doped NiO	Ni	650 °C	H ₂ , CO
PAFC	H ₃ PO ₄	Pt/C	Pt/C	200 °C	H ₂
AFC	KOH	Pt-Au	Pt-Pd	100 °C	H ₂
PEMFC	Perfluorosulfonic acid polymer	Pt/C	Pt/C	90 °C	H ₂

1.2.1 Proton-exchange membrane fuel cell (PEMFC)

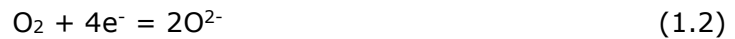
Due to their low operating temperature and the non-corrosive, solid nature of the electrolyte used, PEMFCs are among the most widely used FCs, especially in the electrical vehicle industry. For instance, the commercial Toyota Mirai fuel cell vehicle (FCV) has about 370 PEMFC cells in each model generating electricity to run the car [6]. Furthermore, they are also used for portable electricity generation in off-grid areas.

The core reaction that occurs in the PEMFC is the fundamental exothermic recombination of two hydrogen (H₂) and one oxygen (O₂) molecules to form two molecules of water (H₂O). This spontaneous reaction takes place in 2 opposing porous electrodes (anode and cathode) in three steps as described below [7]:

1. Oxidation of H₂ to form 2 positively charged hydrogen ions:



2. Reduction of O₂ to form 2 negatively charged oxygen ions:



3. And the last step occurs when the negatively charged oxygen ions combine with the positively charged hydrogen ions to create the water molecule:



Thus, the three essential parts of any FC are its cathode and anode with the electrolyte stacked in-between them. To better understand the mechanics of these parts, it is suggested to get familiar with the illustration below (see Fig. 1. 2.) depicting the operation of PEMFC.

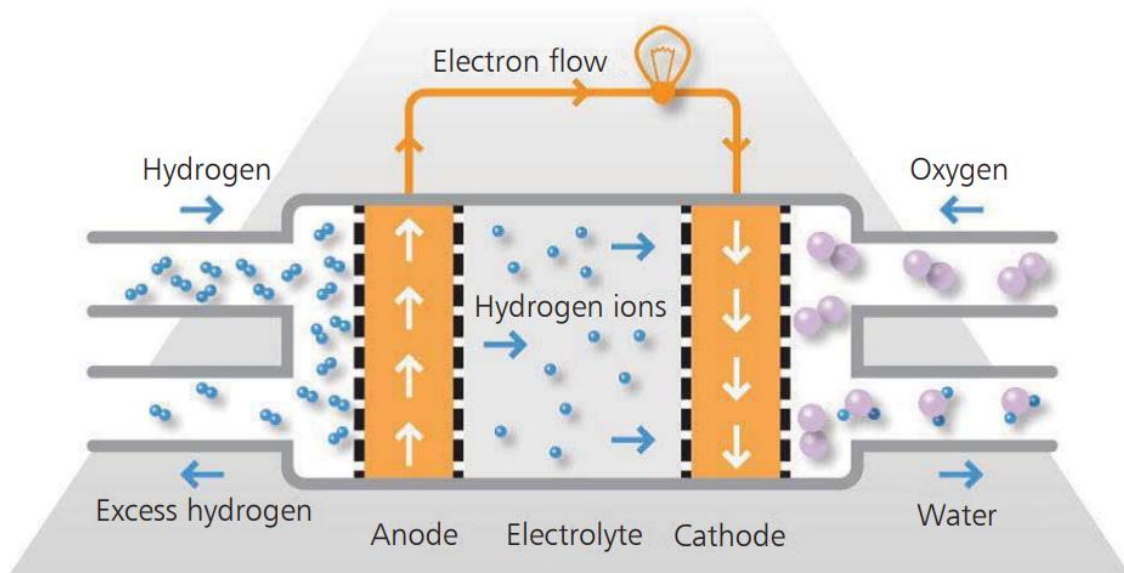


Fig. 1. 2. A schematic of a proton exchange membrane fuel cell [8]

As a low-temperature range FC, PEMFC has a limited option of fuel type (H₂) to be used in the operation. When the hydrogen is fed into the core, it is adsorbed by the anode material and the oxidation (1.1) reaction starts. This results in dissociation of each H₂ molecule into two electrons and two H⁺ ions. Next, with the help of an external electrical circuit, the electrons flow directly to the cathode while the hydrogen ions penetrate through the proton-exchange membrane (PEM) which also acts as an electrical insulator. At the same time, oxygen molecules in the air adsorb to the cathode and are reduced (1.2) by the flow of electrons from the anode. Because the electrons cannot pass through the polymer electrolyte membrane between the anode and cathode, they are

forced to travel through an external circuit where they can be used to do work. Consequently, reduced oxygen atoms and hydrogen ions moving through the electrolyte combine to form water (1.3). The produced water and heat are the only by-products of the PEMFC.

One of the defining characteristics of the operation temperature of PEMFC is the ionic conductivity in the proton-exchange membrane. As the water is required to maintain the ionic conductivity of the membrane, the fuel cell's working temperature is kept below 100 °C to avoid evaporation of the water after its formation [9].

1.2.2 Alkaline fuel cell (AFC)

The AFC is a low-temperature fuel cell technology that has also been used in space applications [10]. The type of electrolyte used in the AFCs is the liquid solution of KOH (potassium hydroxide) which makes its operating principle distinct to PEMFC's [11]. Unlike in the PEMFC, as illustrated (see Fig. 1.3.) on the basic design of the AFC, hydroxyl (OH^-) ions pass through the alkaline electrolyte (instead of protons) where they recombine with hydrogen ions to form water molecules.

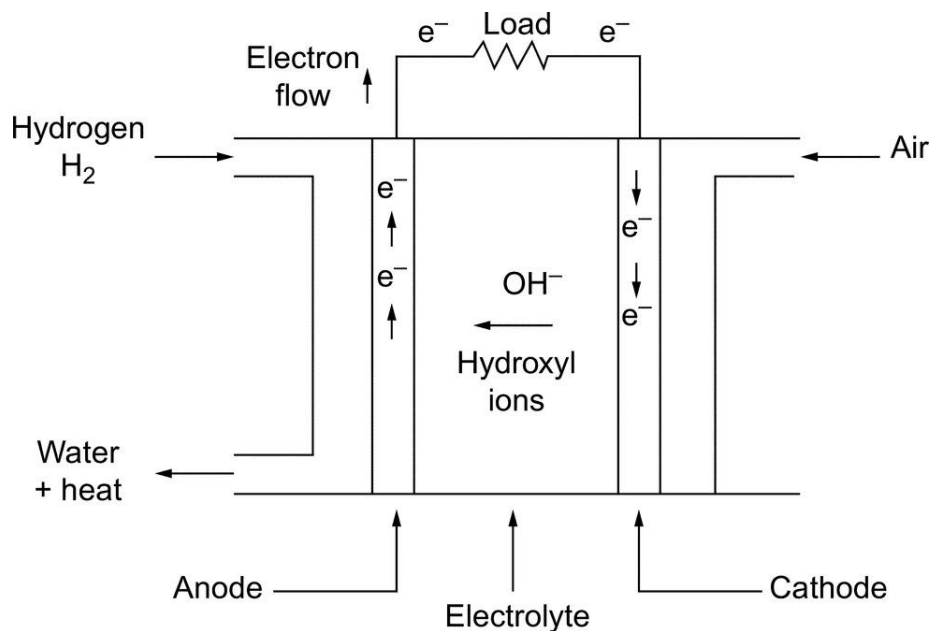


Fig. 1.3. The basic design of the alkaline fuel cell [12]

Thanks to faster kinetics of the ORR in alkaline conditions, the AFCs deliver higher efficiencies than acidic electrolyte fuel cells. However, their power density is significantly lower when compared to the PEMFCs and employing KOH as the electrolyte creates a

constant requirement to maintain the KOH and carbonate (resulting from the reaction with CO₂ in the air) concentration [13].

As a solution to these disadvantages, polymeric anion exchange membrane (AEM) which also use the hydroxide ions as the conductor were introduced to AFCs. This type of fuel cell is commonly referred as the anion exchange membrane fuel cell (AEMFC). In AEMFC, cationic moieties cannot move freely as in the liquid electrolyte (AFCs) and this prevents the creation of carbonate precipitates in the cell [14].

1.2.3 Phosphoric acid fuel cell (PAFC)

The PAFCs are known as the first generation for the modern fuel cells used commercially. As it is obvious from its name, the electrolyte used in the PAFC systems is highly concentrated (>95%) phosphoric acid (H₃PO₄) stacked between the carbon electrodes [15]. Although the occurring cell reactions including the fuel (H₂) and oxidant (air) type are the same with the PEMFC, the PAFCs are required to be corrosion-resistant because of the acidic environment resulting from the electrolyte choice [16]. Optimized operation temperature for these systems ranges between 180 and 210 °C and their carbon monoxide tolerance can reach 1.5% at the anode [17]. The PAFCs exhibit several advantages such as being a mature, reliable, and long-performance technology and their disadvantages include expensive catalysts and corrosive electrolyte usage and vulnerability against CO and S poisoning [17].

1.2.4 Molten carbonate fuel cell (MCFC)

Operating at a high temperature of 650 °C, MCFCs use 2 types (potassium and lithium) of molten carbonates in a mixture as an electrolyte [13]. One special feature of these systems is the capability to carry out internal reforming in which they convert hydrocarbons to hydrogen within the system owing to their high-temperature operation allowing them to perform the reforming without any external reformer. Besides, the MCFCs exhibit better resistance against impurities and CO₂ (or CO) poisoning making them suitable to use coal or carbon oxide derived gases as fuel [16].

On the other hand, the cell life is the system's major drawback due to the intense working environment created by the high operating temperature and the corrosive electrolyte [16].

1.2.5 Solid oxide fuel cells (SOFC)

The highest chemical to electrical energy conversion efficiency rate and the operation temperature (up to 1000 °C) belongs to the SOFCs. As the name suggests, SOFCs contain solid oxide ceramic-derived materials like yttria-stabilized zirconia (YSZ) as the electrolyte and it allows entering oxygen atoms to combine with the electrons (coming from the anode) to produce oxygen ions at the porous cathode [18]. Next, as shown in the schematic (see Fig. 1.4.), the generated oxygen ions pass through the electrolyte to the anode where they oxidize the hydrogen fuel to provide electron flow to through the external circuit and form water as the by-product.

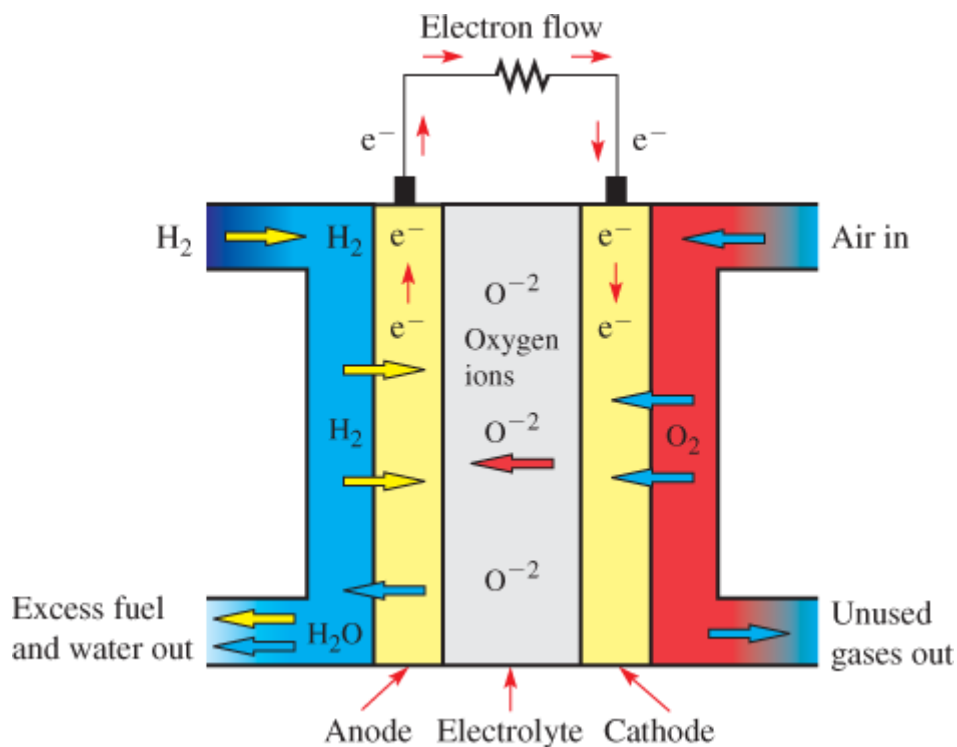


Fig. 1. 4. Operation principle of the SOFC [19]

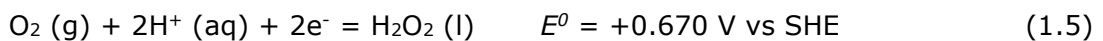
Although the hydrogen is quite practical to be used as a fuel in SOFC, alternative hydrocarbon fuels are preferred due to several advantages [18]:

1. Fuels like methane, propane or biofuels can be potentially used directly at the anode without being restricted to the purified hydrogen (which is not possible with PEMFCs)
2. The reaction between the hydrocarbons and air (or steam) which produces hydrogen and carbon monoxide is not hard to conduct
3. This internal reforming process can exhibit high thermodynamical efficiency

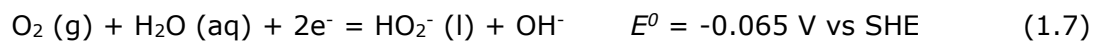
1.3 Oxygen reduction reaction

The oxygen reduction reaction occurs in several crucial reactions in different domains ranging from biological respiration to electrochemical energy conversion in fuel cells. As oxygen is the common oxidizer for many technologies including the fuel cells, understanding the properties of ORR is important to ensure effective and smooth reaction at the cell's cathode. In aqueous solutions, the oxygen reduction reaction can take place either by direct four-electron transfer (in which O_2 is reduced to H_2O) or two-electron transfer (where O_2 is reduced to H_2O_2 which in turn can be reduced to water or OH^-) [20]. As the potential (ΔE) value varies based on the pH environment of the reaction (acidic or alkaline), it is possible to write the two pathways for ORR reaction as given below [21]:

1. In acidic ($pH = 0$) media:



2. In alkaline ($pH = 14$) media:



In these equations, (g), (aq), and (l) refer to the gas, aqueous and liquid phases respectively and SHE stands for the „standard hydrogen electrode“ which acts as a reference potential.

1.3.1 Kinetics of ORR

One of the most important requirements for fast processing reaction is the proximity of the reaction potential to the thermodynamic potentials which is achieved by fast charge transfer kinetics. Unfortunately, for ORR in fuel cells, this is an issue as it has been reported that its kinetics exhibit an overpotential η and are thus slow [22]. This overpotential can be expressed via the given equation:

$$\eta = E_r - E_{eq} \quad (1.8)$$

Here, the difference between E_r (the resultant potential) and E_{eq} (the equilibrium potential) is called the polarisation which can be divided into three parts as follows:

$$\eta = \eta_{\text{act}} + \eta_{\text{conc}} + iR \quad (1.9)$$

In this equation, η_{act} is the activation overpotential characterizing the charge transfer kinetics of the reaction and it is always present especially in smaller polarisation currents. However, the concentration overpotential (η_{conc}) is present in larger polarisation currents and it describes the mass transport limitations. The third parameter is the ohmic drop (iR) that denotes to the electrolytic resistivity in the electrochemical reaction [22].

The contribution of these overpotential parts to the overall polarisation curve is shown in Fig. 1.5. below. The graph shows the relationship between the cell voltage (V) and the current density ($\text{mA}\cdot\text{cm}^{-2}$) which is also important to evaluate the performance of the given cell.

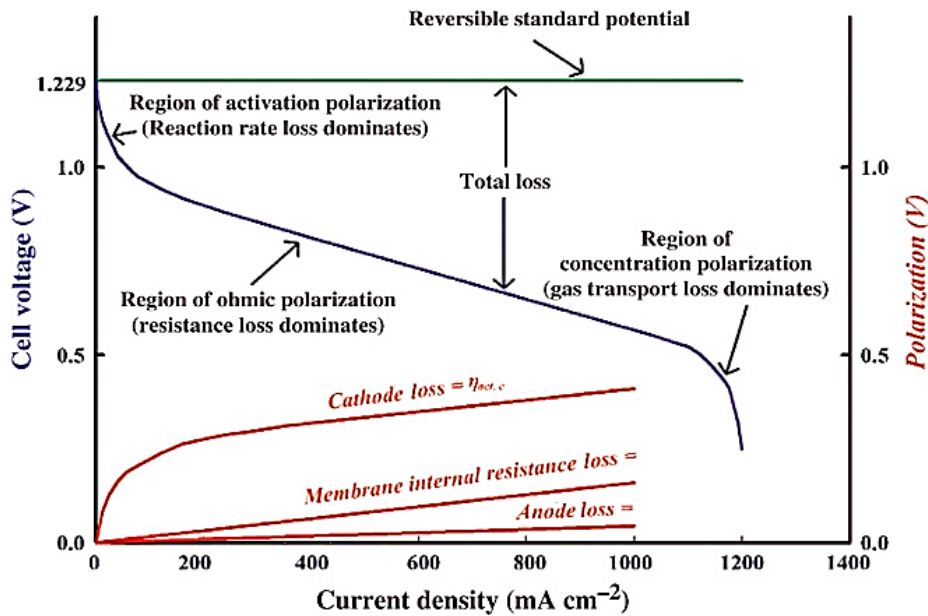


Fig. 1.5. Polarization curve of PEMFC [23]

1.3.2 Pt-based catalyst materials used in the ORR

Due to its slow kinetics (which is more than six orders of magnitude slower than the HOR at the anode in acidic conditions) [24], [25] of the ORR half-reaction, the catalyst is an inevitable part of the fuel cells. To maintain desired activity and operation efficiency, there are several requirements for catalyst materials to comply with [8]:

1. To enable the reaction, the catalyst must be able to adsorb the reactant strongly while avoiding any catalyst surface blockage caused by very strongly adsorbed intermediates or products as stipulated by the Sabatier principle [21]

2. It must be selective to develop only the desired substances with minimum side products
3. Stability is another important factor to consider for the catalyst as it must tolerate the presence of harsh environment (strong oxidants, fluctuating temperatures, reactive radicals, etc.) in the fuel cell operation
4. The catalyst needs to be resistant to poisoning from gas and fuel cell impurities

In case of PEMFCs, the platinum catalyst is considered to perform better than other alternatives with regard to the requirements listed above, namely based on its performance in activity, selectivity, and stability as a catalyst [8]. Naturally, other noble metal alternatives also exist as a catalyst for ORR purposes, however as it can be seen from Fig. 1.6. Pt exhibits superior catalytic activity with regards to other metal species and that is the main reason why it is a common material employed in the industry.

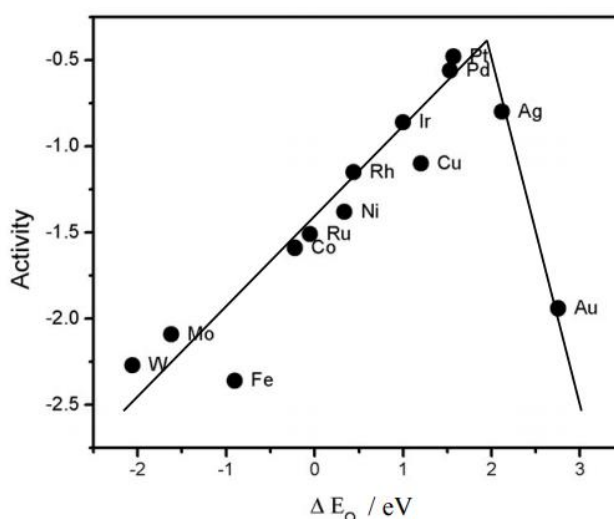


Fig. 1.6. Trends in oxygen reduction activity plotted as a function of the oxygen-binding energy and OH binding energy, Copyright 2004 American Chemical Society [21]

The modern Pt-based electrocatalysts used in the PEMFC systems (in both electrodes) are Pt or Pt-alloy nanoparticles (NP) scattered (see Fig. 1.7.) on a support material such as carbon black [26]. Catalyst material with this kind of structure (platinum scattered on carbon) is often abbreviated as Pt/C.

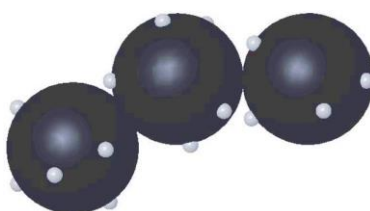


Fig. 1.7. The idealized structure of carbon-supported platinum catalyst for PEMFC [27]

As it can be obvious from its name, the support material supports the catalyst to achieve properties like high surface area, corrosion resistance, electronic conductivity, and chemical inertness which are essential for efficient operation [28]. Furthermore, the presence of carbon as the support material allows easier recovery of precious metal by burning the carbon and it is possible to tune the morphology of the carbon for different applications. Apart from carbon black, there are several other carbon support materials that are researched for fuel cell applications such as graphene, carbon nanofibers, carbon nanotubes, carbon shells, etc [26]. However, the most commonly used carbon black support material is Vulcan XC-72 which was first used in PAFC catalysts and acts as a good catalyst material for PEMFC as well [29].

1.3.3 Alternatives to the Pt-based catalyst materials

Despite their desirable catalytic activities, current Pt-based materials are still not the ideal catalysts because of their limitations such as rarity, high cost, carbon monoxide poisoning, etc. That is why achieving efficient catalysts with minimal Pt loading or developing alternatives that do not require precious metal contribution is essential.

With properties like large surface area, flexible morphology, and adequate conductivity, carbon-based materials are presented as an alternative to the metal-based catalysts [25]. Some of these materials even surpassed the benchmark of Pt/C materials with regards to their ORR activity at the same loading mass as shown in the polarization curves (see Fig. 1.8.) below. Another promising candidate to replace the Pt-based catalysts is the non-noble metal-based catalyst of nitrogen-coordinated iron on carbon support (Fe-N-C) which has also been reported to exceed the results of commercial Pt/C in terms of their higher onset and half-wave potentials [30].

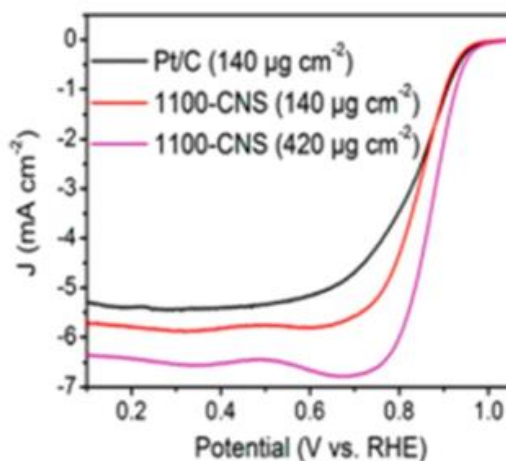


Fig. 1.8. Polarisation curves of the carbon-based catalyst samples and commercial Pt/C [25]

1.3.4 Pre-treatment of carbon black

Despite the extensive use of carbon black as the support material for Pt-based catalysts, there is still room for developing its characteristics to better suit the purpose. To achieve catalyst nanoparticles within the desired size range, electrochemical activity, and surface area properties, carbon materials can be chemically treated prior to modification with platinum nanoparticles. This often includes dispersing the sample in an acidic (or peroxide) medium and refluxing the mixture (so that it does not evaporate above the boiling point) at high temperature for a long period to introduce surface functionalities. The type of medium used in this procedure determines the number and nature of the oxygen functional groups on the surface of the treated carbon. For example, treatment in acidic media can decrease the hydrophobic behavior of carbon and result in a better interaction between the carbon material and aqueous metal precursor. It has been reported that heat pre-treated carbon black samples have shown to decrease the Pt NP size, thereby increasing the utilization of Pt and the overall ORR activity when compared to commercial alternatives [31].

1.4 Pt/C synthesis methods

As the primary type of carbon black used in this study is Vulcan XC-72R, synthesis methods associated mainly with this type of carbon will be discussed.

Two main techniques used for carbon-supported nanoparticle synthesis are physical and chemical methods [32]. The chemical technique has certain advantages including the possibility of controlling the nanoparticle size, shape, and composition properties. This is quite important as it can also be seen from Fig. 1.9. below, shape and size-controlled particles exhibit high levels of ORR mass activity and mid-range specific activity in the measurements.

Thus, it is evident that by efficiently adjusting the shape, size, and other factors, a final catalyst material with superior ORR properties in contrast to the commercial Pt/C can be prepared which in turn means either reduced PGM loading or improved catalytic activity with the same loading. That is why choosing the most suitable synthesis method and defining a benchmark value for the size and shape of the particles are essential experimental goals.

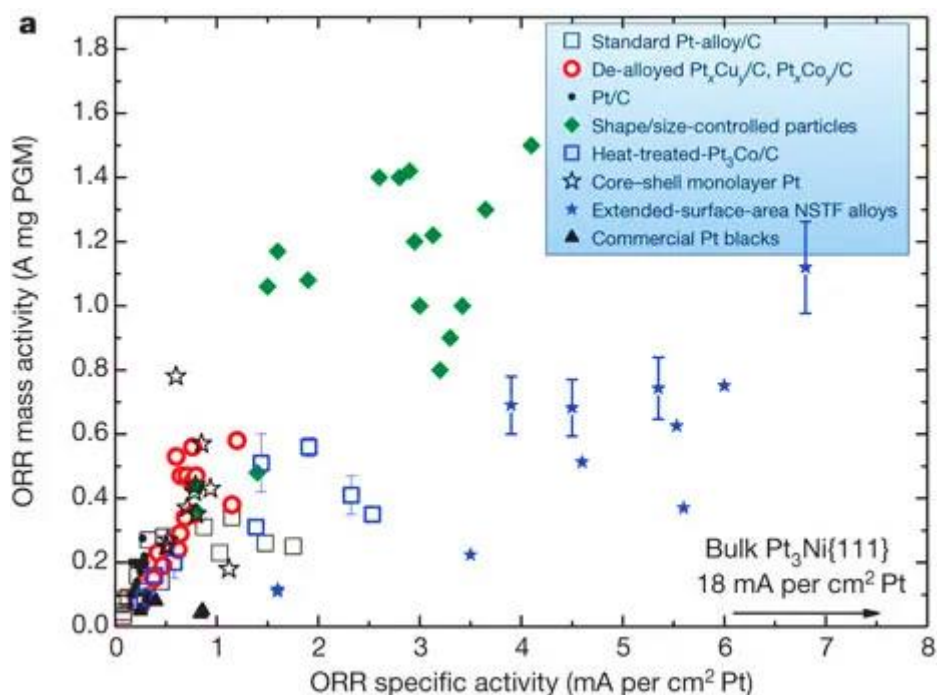


Fig. 1.9. Kinetic activities of different Pt-based electrocatalysts measured by rotating disc electrode (RDE) at 0.9 V vs. Reversible Hydrogen Electrode (RHE) [33]

The synthesis methods that require a support material for the process are referred as the *in-situ* methods in the library. These include techniques [34] such as:

- wet chemistry impregnation
- electrodeposition
- polyol processes
- hydrothermal methods

The choice of carbon is crucial, as it acts not only as a carrier, but also affects the dispersion and stability of the metal particles which dictates the final activity and durability of the electrocatalyst [35].

1.4.1 Comparison of various chemical synthesis methods

To identify the most appropriate synthesis technique for the desired application, it is important to make a comparison of their advantages and drawbacks as given in Table 1.2.

Table 1.2. Advantages and disadvantages of three in-situ synthesis methods

Synthesis method	Advantages	Disadvantages
Impregnation [32]	Simple, environmentally friendly, low energy consumption	Hard to control nanoparticle size and distribution
Electrodeposition [36]	Loading in microgram range is possible	Further deposition increases the metal particle size on the substrate
Polyol [32]	Possible to achieve particle size of 1.8 – 4.7 nm. Scaling-up is easier due to the low-cost and simple process	Thermodynamically unfavourable (heating required)

It is clear from the table that the impregnation method can be used in instances that do not rely much on NP size and distribution factors owing to its simple two-step process that proceeds in low temperature. In this synthesis method, a homogenous mixture is achieved by immersing the metal precursor in aqueous solution with carbon black which is then reduced in either liquid or gas phase with the help of reductive agents such as $\text{Na}_2\text{S}_2\text{O}_3$, NaBH_4 , $\text{Na}_4\text{S}_2\text{O}_5$, N_2H_4 , and hydrogen respectively [37].

In case of the electrodeposition method, several different procedures are employed including the 'through-membrane' deposition in which positively charged platinum precursor diffuses through the thick exchange membrane and the direct deposition occurs when the platinum particles form a thin layer on the previously wetted carbon black substrate by applying the current pulse electrodeposition [38]. This synthesis method allows precursor loading on microgram range accuracy; however, it is limited by a drawback as after the initial deposition, following metal particles are deposited on the initial particle causing an increase in the particle size [36].

For the polyol synthesis method, polyalcohols like ethylene glycol, propylene glycol, diethylene glycol, and benzyl alcohol with high boiling temperatures are used both as a solvent and stabilizing agent for particle growth and nucleation control [32]. It was first developed by Figlarz et al. in 1988 for synthesizing metal powders such as Ni, Cu, and Co [39]. This process is also used in the synthesis of metallic, semiconductor and oxide NPs and it involves the dissolution of the metal precursor (usually salt) in a glycol (see Fig. 1.10.) and increasing temperature of the solution while refluxing [40].

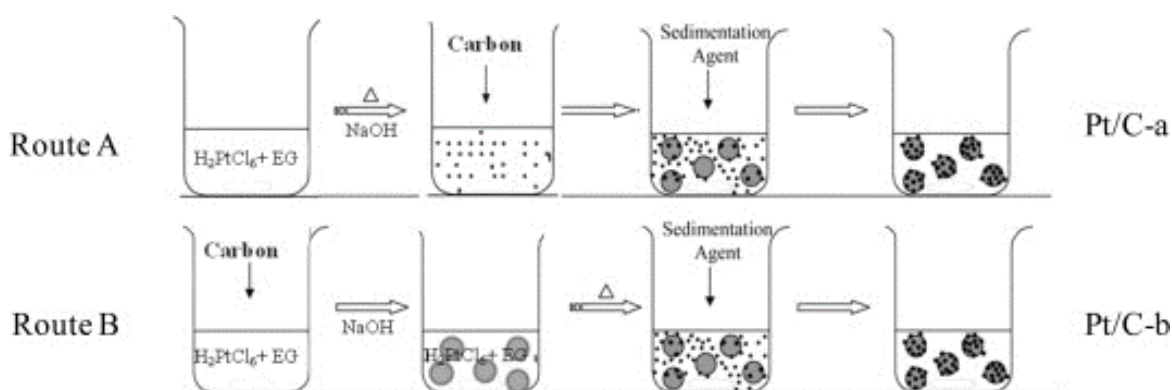


Fig. 1.10. Schematic of two typical polyol routes used for Pt/C nanoparticle synthesis [41]

Obviously, due to the thermodynamically unfavorable dynamics of the process, in some cases, the heating can take up to several hours. However, as the boiling temperature of the polyols used ranges between 473-593 K, the synthesis can proceed without the presence of high pressure and autoclave [42]. Furthermore, other advantages [42] such as polyol's chelating ability (which controls the particle agglomeration, growth, and nucleation) and its reductive ability at high temperatures (prompt reduction of the metal precursor to NP form) makes it a fitting process to achieve the metal NPs with the desired size and properties for catalyst purposes.

1.5 Summary of the literature review and aim of the study

Although fuel cell technology has the potential to pave the way for green energy systems, the industry is still challenged with a major bottleneck of the expensive Pt-based catalysts used to accelerate the core oxygen reduction reaction. However, there are several promising solutions that may bring improved economical and technological viability for the fuel cell systems. One of these solutions is to cut the cost by reducing the amount of platinum used in these catalysts without compromising the electrochemical activity of the material and even increase it in some cases. This is accomplished by using support materials such as carbon black to increase the utilization of Pt by increasing the available Pt surface area while decreasing the mass of Pt needed. Moreover, it is also possible to take the extra step and apply pre-treatment to the carbon black material in order to further increase the activity of the catalyst material towards the ORR and improve its electrochemically active surface area (EASA) by controlling the nanoparticle size of the final sample [31].

A comparison of various synthesis methods was also discussed in the review and it was concluded that the polyol method is the most suitable for the purpose of this work as it is possible to reach NP size within 1.8 to 4.7 nm and avoid agglomeration of the particles with this process [32]. Thus, it is assumed that the synergy of carbon black pre-treatment and polyol synthesis method may result in higher mass and specific activities for ORR. This is quite important because it has been shown (see Fig. 1.9.) that heat-treated and size-controlled samples surpass the commercial Pt/C in terms of electrochemical activity.

This work aims to find the optimal material that exhibits the desired catalytic activity, NP morphology, and EASA among the Pt catalysts with Vulcan carbon as the support material. To do this, first, the Vulcan carbon is pre-treated via different pathways, and the effect of pre-treatment on the final Pt/C sample is examined. Next, N-doped carbon is used as the support material and analyzed in the same way. Finally, all the samples are compared among one another to detect the method that fits the purpose of the work the most.

2. EXPERIMENTAL

2.1 Pre-treatment of carbon black

For pre-treatment of the carbon black (C), Vulcan XC-72R (shortly XC) from The Fuel Cell Store (USA) was used as delivered in the powdered form and with the average particle size of 50 nm. The procedure was conducted according to the instructions given in the source paper [31]. Two chemical pre-treatment pathways (with 65% nitric acid from Sigma-Aldrich, Germany, and 30% hydrogen peroxide from Lach-Ner, s.r.o., the Czech Republic that were not processed further) were used in this work. The only difference between these two methods is the type of medium that the XC was dispersed in. Before the pre-treatment, three-neck round bottom flask was washed with the so-called Piranha solution to ensure clean glassware. Then 0.5 grams of the XC were dispersed in 500 ml of 5% HNO₃ (and 10% H₂O₂ for the next experiment) and refluxed (see Fig. 2.1.) with a temperature ranging from 80 to 110 °C for about 18 hours overnight. Next, the mixture was cooled in room temperature, washed with a continuous flow of Milli-Q® water for 20 minutes and filtered with PTFE membrane. As the last step of the pre-treatment, the XC was dried in an oven (PEAKS PCD-C6(5)000/China) at 105 °C for about 12 hours.

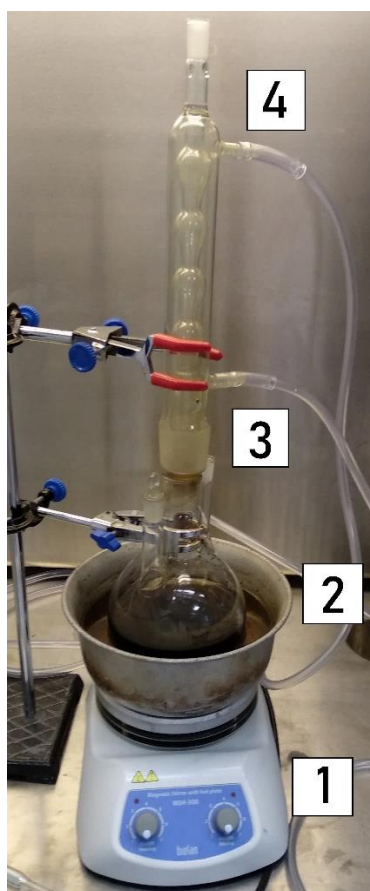


Fig. 2.1. A typical reflux set-up. 1-Heater, 2-Oil bath, 3-Water inlet, and 4-Water outlet

2.2 Synthesis of the catalyst

2.2.1 Pt/XC polyol synthesis protocol

The materials used for this synthesis were following: Ethylene glycol (99.5%), NaOH (98%, from Sigma Aldrich, Germany), dihydrogen hexachloroplatinate (IV) hydrate (99.9% metal basis, from Alfa Aesar, USA), acetone and Milli-Q® water (from Merck Millipore, USA). They were all used without further processing.

First, 40 ml of ethylene glycol (EG) was taken and measured (CyberScan PC 510 pH meter) to find the initial *pH* (~7). Then, to achieve a *pH* level of 11, about 0.4 ml (with 0.1 ml drops) of 1 M NaOH was added to the EG. Next, 0.25 grams of the pre-treated XC was mixed with 15 ml of the *pH*-adjusted EG and stirred (with magnetic bar) under N₂ for 1 hour. To get 20% loading of Pt on XC (1:4 Pt to XC ratio), 62.5 mg Pt was required. Considering the molar mass ratio (~2.1) of Pt to chloroplatinic acid hydrate H₂PtCl₆, 131.25 mg (62.5*2.1) of H₂PtCl₆ in crystalline form was measured and diluted to 17 ml of Milli-Q water. After adding the diluted platinum precursor solution to the EG-XC mixture, it was refluxed for 3 hours at 115 °C under N₂ flow. As the last step of the synthesis, the refluxed mixture was stirred overnight under N₂ and washed with a continuous flow of Milli-Q water (and with acetone for a very short period) after which the sample was dried in an oven for 3 hours at 110 °C.

2.2.2 Pt/N-doped XC polyol synthesis protocol

Doping procedure - The materials used for doping were the following: Vulcan XC-72R from The Fuel Cell Store (USA), PVP (Mv-40,000), DCDA, ethanol (100%, from Chem-Lab, Belgium). It has to be noted that for N-doped XC synthesis, the Vulcan carbon was not pre-treated prior to nitrogen doping, and the other materials were used as received. N-doping was performed according to a procedure described in [43].

For doping, 0.4 g of XC was mixed with 0.04 g (10 times less than XC) of PVP powder and 8 g (20 times more than XC) of DCDA. After adding ethanol to the mixture in an Erlenmeyer flask, it was sonicated in an ultrasonic bath for 1.5 hours. Then, the mixture was dried at 75 °C for about 1 hour and 20 minutes. Next, a quartz boat was used to put it in an oven and purged with N₂ flow for 15 mins prior to activation at 800 °C (heating rate of 10 °C/min) for 2 hours under N₂. After cooling down the oven to room temperature, the sample was taken and measured. The polyol synthesis process for N-doped XC was the same as the other Pt/XC samples written in the previous item.

2.3 Characterization techniques and equipment

2.3.1 Electrochemical characterization

For electrochemical characterization, hydrodynamic voltammetry techniques of RDE (Rotating Disk Electrode) and RRDE (Rotating Ring-Disk Electrode) are commonly used in the experiments. By using these techniques, it is possible to achieve steady-state, controllable diffusion conditions which enable precise measurements, smaller mass transfer contribution to the overall reaction, and minimal double layer charging current [44].

RDE - In case of the RDE, the spinning of the working electrode in the electrolyte drags the reactant to the electrode surface while the products are flung away from the surface [45]. Side and top views of the RDE mechanism are shown below in Fig. 2.2.

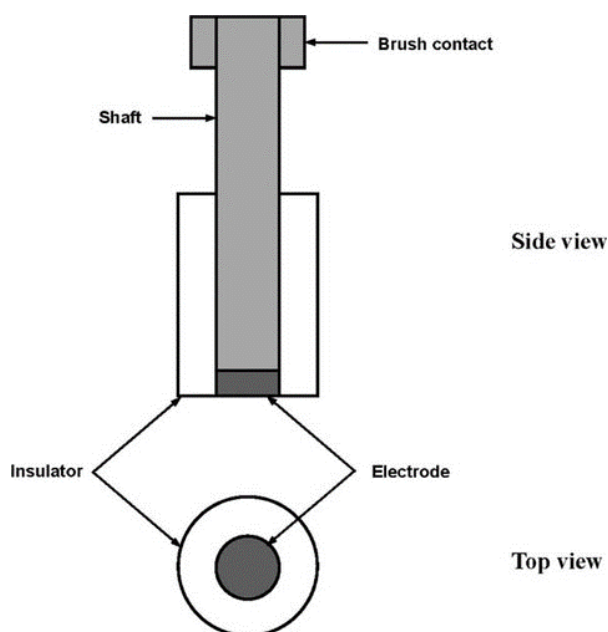


Fig. 2.2. Schematic representation of a rotating disc electrode (RDE) [44]

Starting from the top, the brush contact is used for electrical connection while the working electrode is mounted to the shaft which is rotated by a motor. In the picture, the black circular disk surrounded by the insulator material is the surface of the electrode.

Ink preparation and coating - To prepare the catalyst ink for RDE measurement, 1 mg of the catalyst sample powder was mixed with 0.405 μl of Nafion (5%), 250 μl of isopropanol (from Stanchem Sp. z o.o, Poland) and 750 μl of Milli-Q (1:3 alcohol to water ratio) water. Then, the mixture was sonicated for 1 hour at a temperature of < 40 $^{\circ}\text{C}$. Before ink deposition, the electrodes were polished with 1.0 and 0.30 μm alumina

paste slurry (from Buehler, USA) in a figure-eight motion to ensure a uniform surface to a mirror finish. The polished electrodes were first sonicated in isopropanol (5 mins) and then in Milli-Q water (5 mins) to remove alumina residues. The prepared ink was deposited (see Fig. 2.3.) to the electrode surface in three steps of 10 μl (30 μl in total to achieve Pt loading of 30 μgcm^{-2} on the glassy carbon surface) via drop-casting method with a pipette. Between the steps, the electrode was dried in an oven and the ink was sonicated.



Fig. 2.3. Catalyst ink deposited to the electrode surface for RDE test

Cyclic voltammetry (CV) measurements – The CV measurements were conducted in a conventional three-electrode system (see Fig. 2.4.) at room temperature and 0.5 M H_2SO_4 (98%, from VWR Chemicals) solution was used as the electrolyte. The potentiostat (Interface 1010E or Reference 600+ of Gamry instruments from USA) was controlled by Gamry software with Saturated Calomel Electrode (SCE) and platinum wire as reference and counter electrodes respectively. It must be noted that all of the following potential values in this work were converted to Reversible Hydrogen Electrode (RHE) potential by adding 0.244 V to the potential values obtained vs SCE. The working electrode was composed of a glassy carbon with the surface area of 0.2 cm^2 modified with the selected catalyst.

1. The first part of the CV was carried out in order to investigate the EASA of the samples. However, prior to this experiment, the cell was purged with N_2 for 25 mins and later the sample was activated by applying 100 potential cycles in the voltage range of -0.2 V to 1.2 V vs SCE at the scan rate of 500 mVs^{-1} under N_2 flow. After the activation, the voltage range was kept the same (-0.2 V to 1.2 V) and the CV was performed in two different scan rates of 100 mVs^{-1} and 10 mVs^{-1} with N_2 -saturated electrolyte.

2. With the second part of the measurement, the goal was to analyze the degradation and ORR properties of the samples. The cell was purged with O₂ for 25 mins before starting the experiment. To research the aging profile of the samples, first, they were cycled for 500 times with the voltage range of -0.2 V to 1.2 V vs SCE at 500 mVs⁻¹ under the O₂ atmosphere. In this case, the first and final CV curves were obtained to compare the characteristics of the samples after being exposed to 500 potential cycles. Next, the voltage range was adjusted to -0.2 V to 0.8 V in order to conduct the ORR kinetics experiment at 10 mVs⁻¹ with O₂ flow. For this part of the measurement, electrode rotation was applied with changing RPM (Revolutions Per Minute) levels between 400 and 4400.

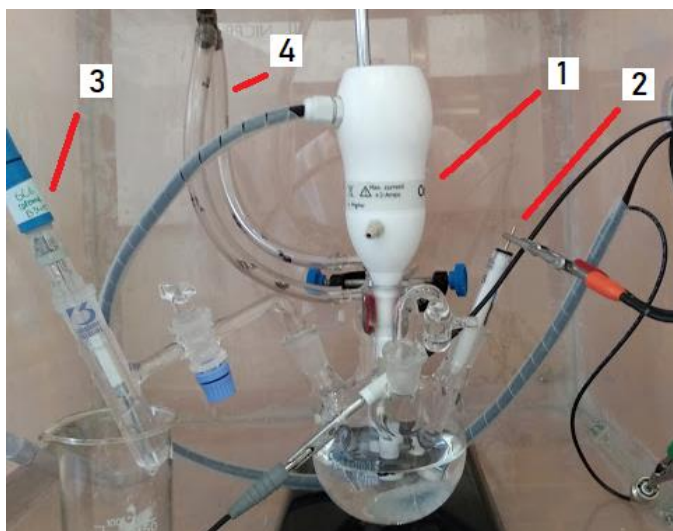


Fig. 2.4. Three-electrode cell: 1-Motor attached to the working electrode, 2-Pt wire as the counter electrode, 3-SCE as the reference electrode and 4-gas inlet for purging/saturation

2.3.2 X-ray diffraction (XRD)

X-ray diffraction is an analytical technique used for characterizing mono or polycrystalline materials by directing X-rays to the desired sample and collecting data from the scattered beams. The obtained peaks are then assigned to reflection planes which define the material's crystal structure and the peak values can also be used to calculate approximate crystal size.

In this work, XRD measurement for all samples was performed with X'Pert³ Powder system by Malvern Panalytical at 40 mA and 45 kV.

2.3.3 Scanning electron microscopy (SEM)

SEM is a surface characterization method using an electron beam to interact with the material surface and obtain signals that can be read as valuable data for creating a topographic image of the sample. During the measurement, electrons generated from the electron source pass through an electromagnetic lens which can be used to control the electron path by changing the current value applied. In this case, two main categories of electrons are present: backscattered (BSE) and secondary electrons (SE).

BSE are produced from elastic interactions with the material and reflected back while SE are generated by atoms of the material due to inelastic interactions. As elements with higher atomic number produce more BSE than lower atomic number elements, a distinction between heavy and light elements can be made based on the brightness level.

To obtain microimages of Pt/XC-72R (H₂O₂ treated), FEG (field emission gun)-SEM was employed operated by Zeiss Ultra 55. Additionally, Energy-dispersive X-ray spectroscopy (EDX) spectrum was also acquired to study the composition of the sample in more detail. The measurement and analysis were performed by Dr. Valdek Mikli (Tallinn University of Technology).

2.3.4 Raman spectroscopy

Raman spectroscopy is one of the common non-destructive techniques for studying the chemical structure of a given sample. For this measurement, incident light generated by a high-intensity laser is directed to the sample, and molecules present in material scatter this incident light mostly without changing its wavelength which is called the Rayleigh scattering. However, this does not provide the observer with any valuable information about the molecules. At the same time, a minuscule part of the incident light is scattered with changed wavelength based on the molecular structure of the given sample. This is called the Raman scattering and is often composed of some peaks with different intensity and wavelength levels corresponding to molecular bond vibrations assigned to specific bonds such as C-C.

The microstructure of carbon black for each sample was studied using micro-Raman spectrometer Horiba LabRam HR800 with a 532 nm laser line for investigating the defective nature of the carbon molecules in detail. The measurement was conducted by Dr. Maarja Grossberg from Tallinn University of Technology.

3. RESULTS AND DISCUSSION

3.1 RDE results

3.1.1 Electrochemically active surface area (EASA) determination

In general, four different samples (Pt/HNO₃-treated XC, Pt/H₂O₂-treated XC, Pt/not pre-treated XC, and Pt/not pre-treated XC that was N-doped) were synthesized in this work. The commercial Pt/C with 20% loading from Sigma-Aldrich was used for comparison. To calculate EASA for each sample, the region under the hydrogen desorption peak of the CV curve (see Fig. 3.1. A) was integrated to find the charge associated with the H desorption region. After subtracting the double layer contribution from the integrated region, EASA was determined with the following equation:

$$\text{EASA (cm}^2\text{/g)} = Q_{\text{h.des}} / Q_{\text{ref}} \times m_{\text{Pt}} \quad (3.1.)$$

In this equation, $Q_{\text{h.des}}$ is the charge associated with the H desorption region (mC), Q_{ref} is the charge required for monolayer adsorption of hydrogen on Pt surface (0.21 mC/cm²) and m_{Pt} is the amount of Pt loading on the electrode surface (g) [46]. The result of this calculation is given in Table 3.1. below.

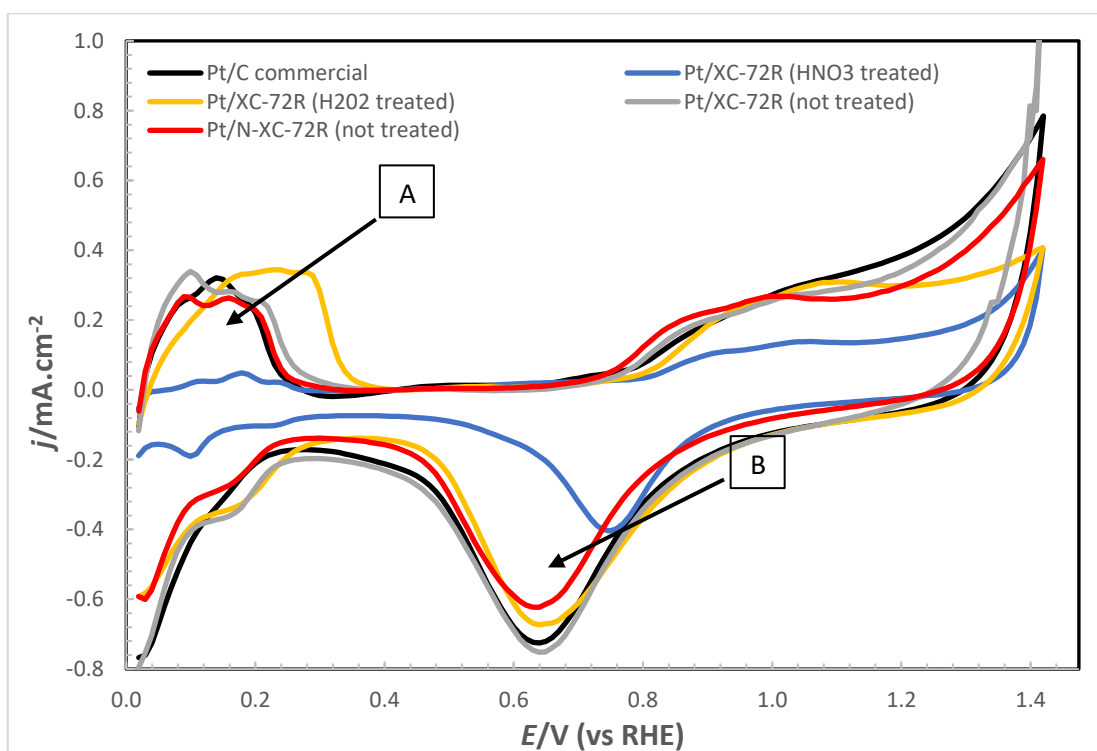


Fig. 3.1. Comparison of cyclic voltammograms for all five samples recorded at 10 mVs⁻¹ under N₂ saturation (0.5 M H₂SO₄) at room temperature. A-hydrogen desorption region and B-oxide reduction peaks

Table 3.1. EASA values for the samples

	Commercial Pt/C	Pt/XC (HNO ₃ treated)	Pt/XC (H ₂ O ₂ treated)	Pt/XC (non-treated)	Pt/N-XC (non-treated)
EASA	77.83 (m ² /g)	13.16	113.88	83.65	65.70

It was found that the electrochemically active surface area of the catalyst with H₂O₂ treated XC was the largest among all the samples and in case of the commercial Pt/C it was about 46.3% larger. However, the effect of pre-treatment on EASA was not observed for the HNO₃ treated sample as the calculated value of this material was the smallest. It should be noted that the calculation was performed with data from the CV at 10 mVs⁻¹ and when the other curve (at 100 mVs⁻¹) was used, there were some differences in the final values including EASA of 40.08 m²/g for HNO₃ treated sample which seems to be a more reasonable result. Even in the second calculation, H₂O₂ treated catalyst had the largest EASA and thus it is assumed that H₂O₂ pre-treatment of Vulcan carbon prior to synthesis results in well-dispersed Pt particles on the support leading to higher EASA values.

3.1.2 ORR activity

To characterize ORR activity, a linear sweep voltammogram (LSV) comparing all the samples at 1600 rpm is given below in Fig. 3.2.

Determining the onset potential for each sample is important to evaluate at which potential the reduction starts to occur. It was found that both hydrogen peroxide and nitric acid treated samples exhibited superior onset potential of 0.95 V and 0.93 V respectively in comparison to the commercial Pt/C (0.89 V) and other catalysts (N-doped XC – 0.90 V and non-treated XC – 0.86 V). This indicates that Pt/XC-72R (H₂O₂ treated) material has the highest catalytic activity towards the ORR and this agrees well with the high EASA value of the same sample. At the same time, diffusion-limited current density (j_{lim} between 0.2 V and 0.7 V, from Levich equation) of this catalyst is around -5.3 mA.cm⁻² which is almost identical to the theoretical value of -5.7 mA.cm⁻² given in the literature [47] and higher than any other sample again meaning a higher electrocatalytic activity. The steep reduction wave of the hydrogen peroxide treated material in the mixed kinetic-diffusion control region (0.2 V < 0.7 V) and its flatter diffusion-limited current density plateau are also associated with favorable ORR properties for the catalyst. Meanwhile, the polarization curve of the HNO₃ treated material was inferior in terms of the gradual reduction wave and smaller diffusion-limited current density.

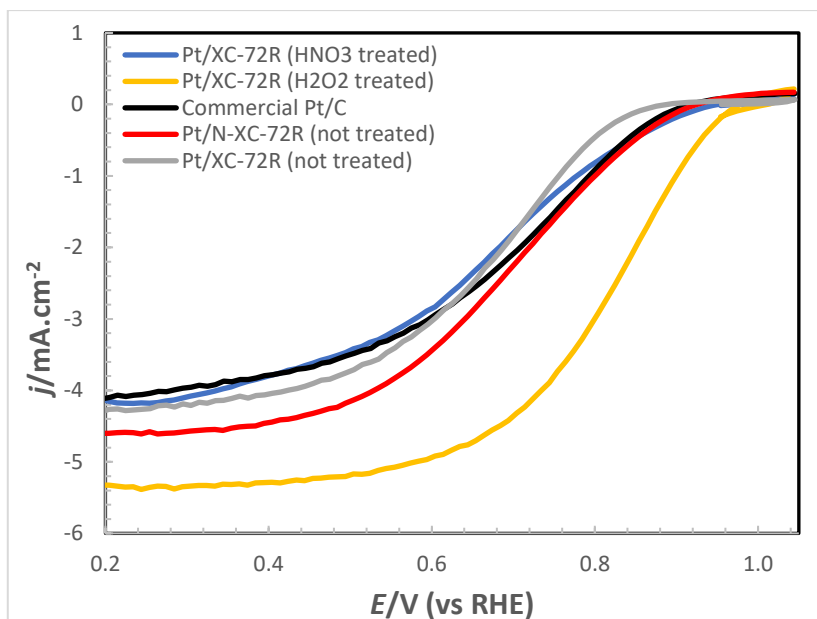


Fig. 3.2. LSVs for all samples (1600 rpm) at 10 mVs^{-1} under O_2 saturation ($0.5 \text{ M H}_2\text{SO}_4$)

On the other hand, there was a minor difference between the onset potentials of Pt/N-XC-72R and commercial Pt/C translating to similar, thus a reasonable catalytic activity for the material. The limiting current density for the N-doped XC sample is slightly higher than the commercial Pt/C which is an advantage. However, in case of the sample with XC that was not exposed to pre-treatment, the onset potential was minimum and there was a shoulder in the mixed kinetic-diffusion controlled region indicating to poorer ORR activity.

The superior tendency of the H_2O_2 treated sample can also be observed in the oxide reduction peaks (Fig. 3.1. B) of CV recorded at 10 mVs^{-1} (double layer charging corrected [46]) in which its current density peak value is almost as high as the commercial Pt/C. The well-defined reduction peaks for all materials occur around 0.65 V except for the nitric acid-treated sample which has a shifted and smaller peak at 0.76 V presumably due to slower oxide reduction kinetics. The activity of Pt/N-XC-72R (non-treated) material was also consistent in comparison to the commercial Pt/C in both CV and LSV curves.

Overall, it is assumed that the type of performed pre-treatment might lead to improved activity in different magnitudes as seen from LSV plots of nitric acid (adequate) and hydrogen peroxide (superior) treated samples. However, it is counter-intuitive to observe that Pt/XC-72R (non-treated) also had similar peak values (current density) to the commercial sample and even slightly surpassing it in case of the oxide reduction peak as shown in Fig 3.1 (B). Thus, further comparison of ORR kinetics for hydrogen peroxide treated and non-treated samples is needed to conclude the effect of pre-treatment on the kinetic activity of the catalyst.

3.1.3 Influence of pre-treatment on the catalytic activity of Pt/XC-72R (H₂O₂ treated)

For a more detailed comparison of the H₂O₂ treated sample with the non-treated material, ORR polarization curves at different rotation rates for both materials are illustrated (see Fig. 3.3.) next to each other.

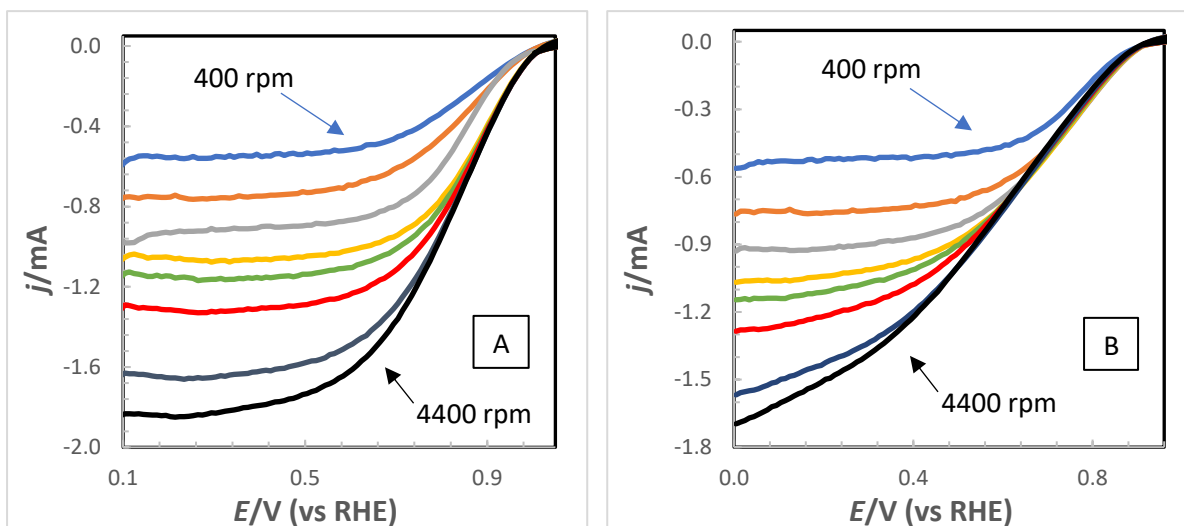


Fig. 3.3. ORR polarization curves of A) Pt/XC-72R (H₂O₂ treated) and B) Pt/XC-72R (non-treated) samples under O₂ saturation obtained at different rotation speeds (0.5M H₂SO₄-10 mVs⁻¹)

Both curves demonstrate a linear relationship between the diffusion-limited current and the rotation rate. However, this is more clearly observed in case of the treated material (see Fig. 3.3. A) in which the flatter diffusion-controlled region is observed in every rotation level with a stable current value indicating better activity. However, the non-treated sample has overlapping curves extending to the diffusion-controlled zone especially at higher rotations and the limiting current stability is almost non-existent in case of the 4400 rpm rotation speed. Slightly higher limiting current values and well-defined plateau of the Pt/XC-72R (H₂O₂ treated) catalyst material can be attributed to a high quantity of oxygen molecule diffusion to the catalyst surface and thus better oxygen reduction characteristics [48]. These results support that hydrogen peroxide pre-treatment of Vulcan carbon may lead to enhanced catalytic activity towards ORR for the final catalyst material. Next, additional discussion on this issue is performed via the Koutecky-Levich analysis.

3.1.4 Koutecky-Levich analysis

To characterize the electron transfer mechanism employed by the catalyst, the Koutecky-Levich (shortly KL) equations are often used to plot the relationship between the reciprocal current density ($1/j$) and reciprocal root of the angular rotation rate ($\omega^{-1/2}$). These equations are as following [49]:

$$1/j = 1/j_k + 1/j_l = 1/(B\omega)^{1/2} + 1/nkC_0F \quad (3.2)$$

$$B = 0.62nC_0F\nu^{-1/6}D_0^{2/3} \quad (3.3)$$

Here, j , j_k , j_l , B and ω are the current density, kinetic limited current density, diffusion-limited current density, Levich constant, and angular velocity, respectively. And n , k , C_0 , F , ν and D_0 denote to the number of electrons in ORR, electron transfer rate constant, the bulk concentration of oxygen, Faraday constant (96485 C), kinematic viscosity and diffusion coefficient for oxygen in the order given.

For sulfuric acid electrolyte, given values [50] are used for the equation (3.3.): $C_0 = 1.1 \times 10^{-6} \text{ mol.cm}^{-3}$, $D_0 = 1.4 \times 10^{-5} \text{ cm}^2.\text{s}^{-1}$ and $\nu = 1.0 \times 10^{-2} \text{ cm}^2.\text{s}^{-1}$.

In a PEMFC system, ORR occurs via two main pathways:

- a. step by step two-electron pathway in which oxygen is first reduced to H_2O_2 by 2 electrons and then to water by further 2 electrons
- b. direct four-electron pathway in which oxygen is reduced to water directly with 4 electrons

To calculate the number of electrons transferred during ORR, intercept, and slope values from the KL plots (see Fig. 3.4.) were used to determine the Levich constant. Next, by considering the corresponding values of kinematic viscosity, bulk concentration and diffusion coefficient of O_2 for sulfuric acid electrolyte, equation (3.3) was employed to quantify the number of electrons involved in the process as below:

$$n = B/0.62C_0F\nu^{-1/6}D_0^{2/3} \quad (3.3.1)$$

This must be noted that the voltage levels (values) used for both of the samples were different based on their ORR polarization curves. However, in order to find the intercept identical voltage value of 0.5 V was chosen for the calculation of n .

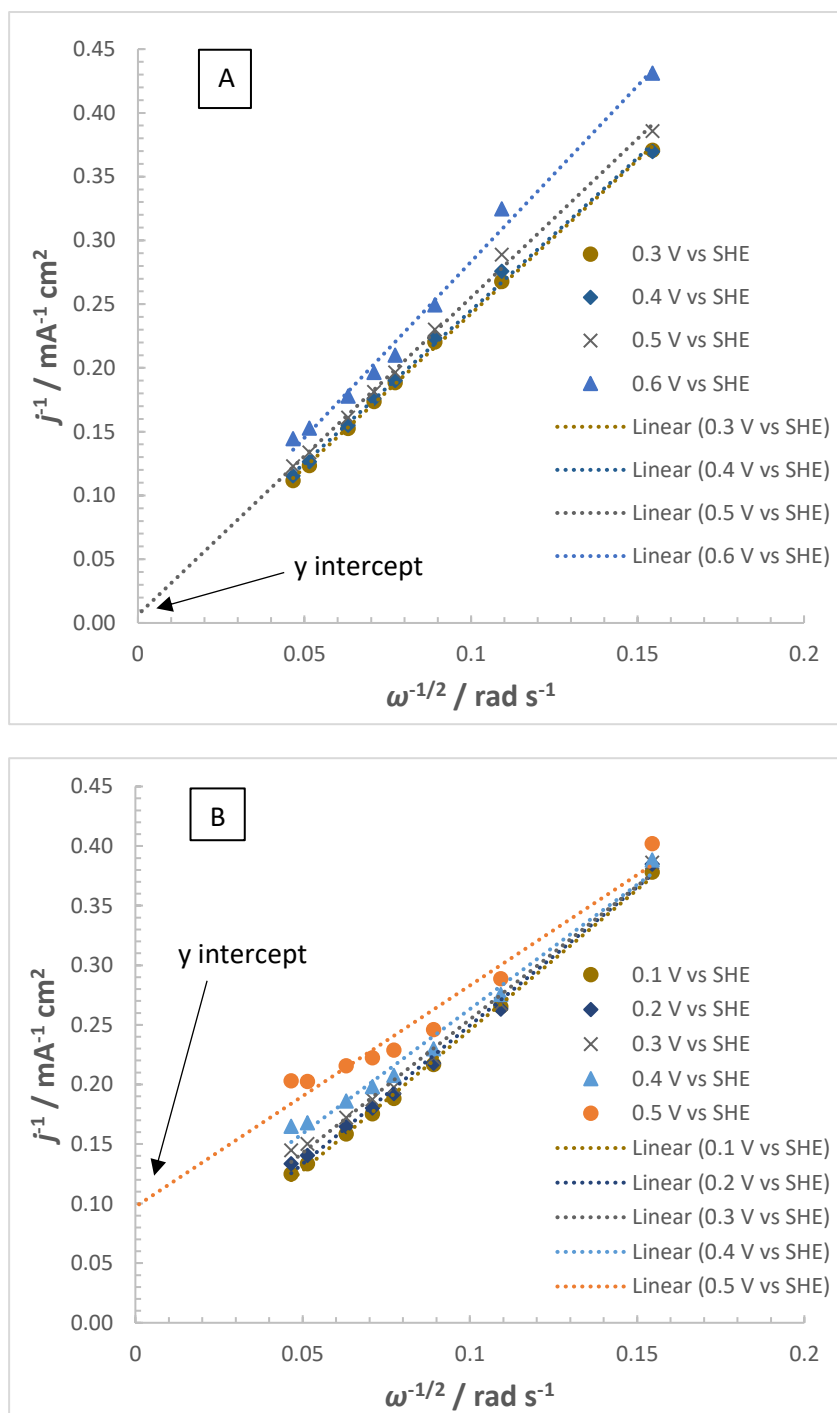


Fig. 3.4. Koutecky-Levich plots of A) Pt/XC-72R (H_2O_2 treated) and B) Pt/XC-72R (non-treated) samples at different voltage and rotation rate values

It was found that n value was around 4.4 for H_2O_2 treated sample at 0.6 V. This is within the commonly referred 10% deviation rate (possibly due to calculation errors) for four-electron transfer pathway and the excess value (~ 0.4) has been reported in other studies [51] as well. Although the transferred electron values were slightly higher (around 5) in case of the non-treated sample, the reduction can still be attributed to the analogical (4-electron) pathway. This suggests that both samples were involved in the direct reduction (b) which is advantageous to the two-electron pathway as the latter results in H_2O_2 formation which is corrosive for the catalyst environment and the oxygen molecule utilization level is higher in case of the direct reduction.

Additionally, KL plots for both materials demonstrate a linear relationship meaning first-order ORR kinetics with respect to the oxygen concentration, however, Pt/XC-72R (non-treated) has a disproportionate and overlapping dependence especially at higher voltage values. Such irregularity might be due to a malfunction during the RDE testing or simply because of the sample's nature. Thus, to draw a conclusion regarding the comparison of KL analysis for these two samples, the y-intercept value (of 0.5 V vs RHE) for both plots (see Fig. 3.4.) has been obtained visually. This intercept figure corresponds to the kinetic current density in the absence of the mass transfer limitations and the results are given in Table 3.2. It must be noted that the rest of the catalyst materials also exhibited a similar linear relationship between j^{-1} and $\omega^{-1/2}$. For comparison, the below table also contains the calculated j_k , E_{onset} , mass, and specific activity [47] (shortly MA and SA) values for all samples.

Table 3.2. Kinetic current density, mass and specific activity values for all samples at 0.5 V

	Commercial Pt/C	Pt/XC (HNO ₃ treated)	Pt/XC (H ₂ O ₂ treated)	Pt/XC (non-treated)	Pt/N-XC (non-treated)
j_k	10 mA.cm ⁻²	5	100	10	9
MA	0.33 A/mg _{Pt}	0.16	3.3	0.33	0.3
SA	428.2 μA.cm ⁻²	1265.8	2926.8	398.4	456.5
E_{ons}	0.89 V	0.93 V	0.95 V	0.86 V	0.90 V

The results reveal that Pt/XC (H₂O₂ treated) sample has the highest kinetic current density at 0.5 V (10 times the commercial Pt/C) while the nitric acid-treated material showed the lowest value (half of the commercial Pt/C). Identically, mass, and specific activity for the H₂O₂ treated is superior to all other samples indicating excellent catalytic activity while the HNO₃ treated sample suffers from surprisingly low values. This encourages the assumption that the type of pre-treatment chosen can affect the tendency of a material to be more active towards ORR and it is possible to conclude that Pt/XC-72R (H₂O₂ treated) catalyst has performed better than the commercial Pt/C sample in almost every approach. However, it is also quite important to investigate the durability of the catalyst in order to evaluate its practical value in a real fuel cell system and this will be discussed in the following part.

3.1.5 Accelerated stress testing (AST) result

Synthesized catalyst materials are often exposed to ASTs to determine their durability and performance in a real system. In this work, 500 potential cycles were applied to all samples, and the differences in the CV curves (see Fig. 3.5.) were observed.

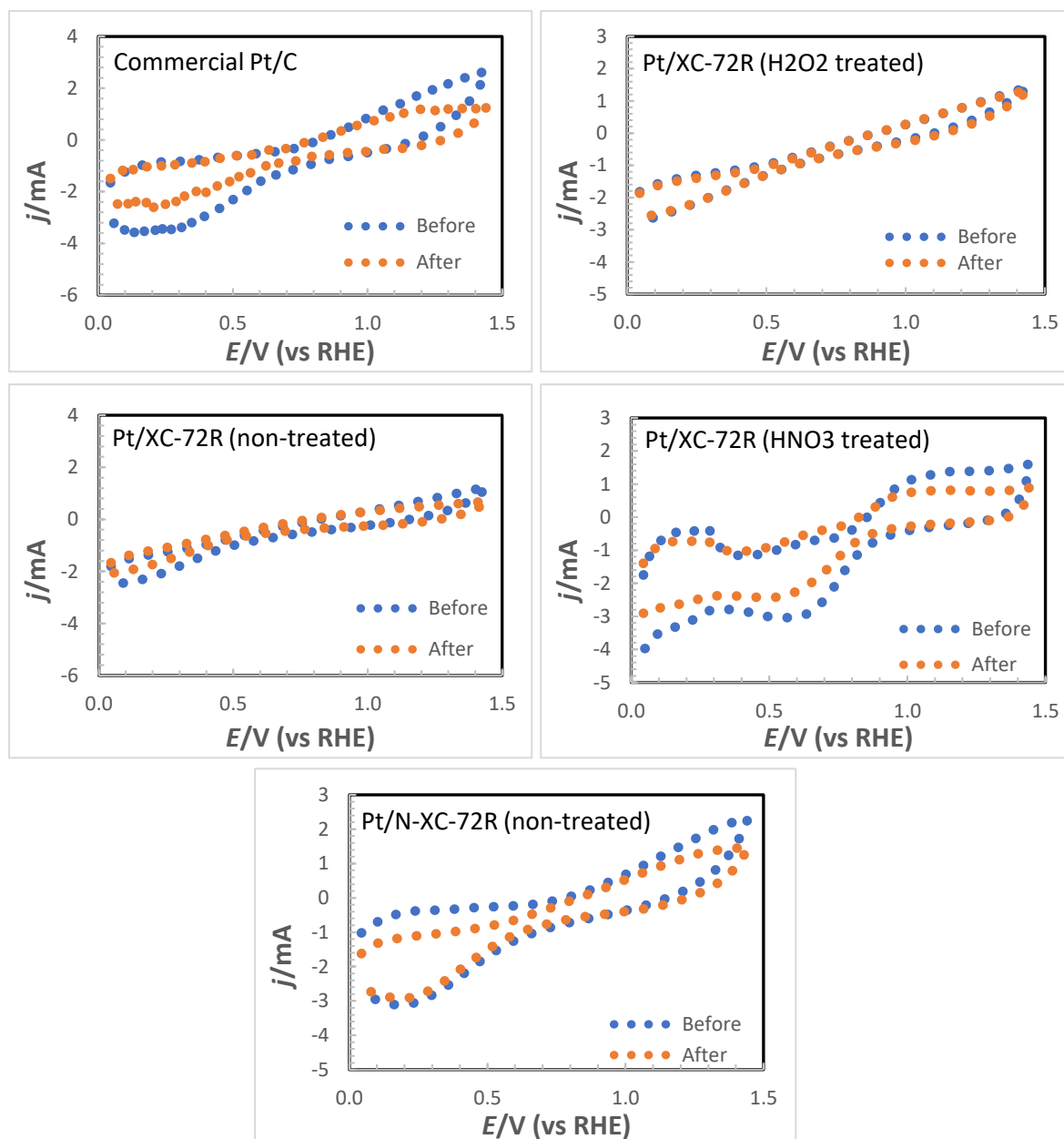


Fig. 3.5. Accelerated stress testing curves for all samples before and after exposure to 500 potential cycles at 500 mVs^{-1} under O_2 saturation ($0.5 \text{ M H}_2\text{SO}_4$)

Among the samples, Pt/XC-72R (H_2O_2 treated) had the most similar cyclic j - E curve in contrast to the result of AST for commercial Pt/C. It was also noticed that there was a shift to lower current values at high voltages for all materials after the cycles. In terms of the catalytic stability among all graphs, the CV curve for H_2O_2 treated catalyst seems

to be barely affected by the stress testing and this suggests that the durability of this material surpasses the rest including the commercial Pt/C. In contrast, Pt/XC-72R (non-treated) has a slightly higher current decrease between the potentials of 1.0 to 1.5 V while N-doped and HNO₃ treated samples exhibit similar and adequate durability.

3.2 SEM images and EDX spectra

Based on the promising and superior results obtained for the H₂O₂ treated catalyst, its morphology was further studied with SEM in order to carry out in-depth analysis as shown in Figure 3.6.

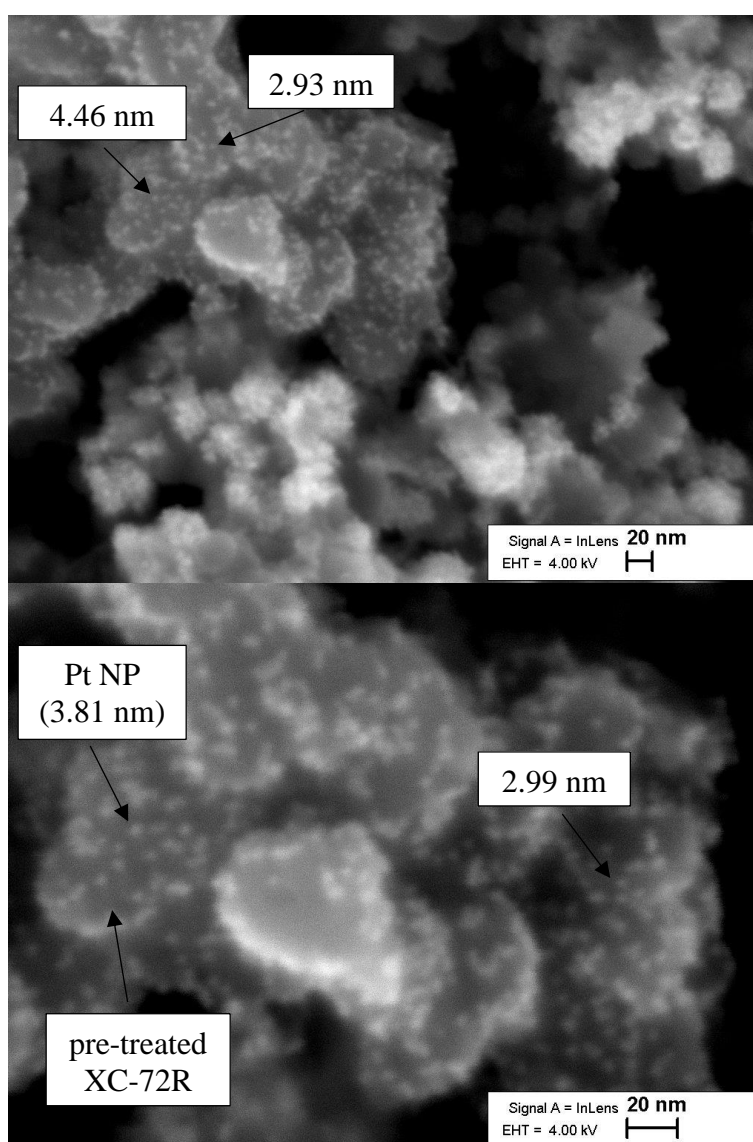


Fig. 3.6. SEM micrographs of Pt/XC-72R (H₂O₂ treated) sample

SEM images reveal that majority of Pt NPs are uniformly distributed over XC-72R. Such distribution is a key characteristic for an efficient catalyst material as this increases the EASA and thus the catalytic activity for ORR. There are also agglomerated Pt sites on the sample however these sites are rather less populated. Hence, Pt utilization seems to be in an adequate level.

Nanoparticle size of Pt was also calculated with the SEM study and it was identified that the value changes between 2.93 nm to 4.46 nm. In another study, Pt NP size of 4.4 nm was suggested as the optimum based on its maximum mass activity and balanced electrochemical stability [52]. Although there are also smaller particles present, the optimal value is almost identical to the NP size (4.46 nm) achieved in this study. This agrees well with the previous catalytic activity results collected for the H₂O₂ treated sample.

On the other hand, the EDX spectrum for both general and Pt-rich areas of the sample was acquired with the data shown in Table 3.3 A and B respectively. The spectrum of the general area confirms the presence of C and Pt in the composition and the stoichiometric ratio of Pt to C (1:4) used in synthesis. In case of the Pt-rich area, the weight amount of Pt is about 53% more than the carbon amount.

Table 3.3A. General EDX spectrum

	Series	unn. C [wt. %]	norm. C [wt. %]	Atom. C [at. %]	Error [%]
Carbon	K-series	82.92	82.93	98.75	1.5
Platinum	M-series	17.07	17.07	1.25	0.7
Total		100	100	100	

Table 3.3B. Pt-rich area EDX spectrum

	Series	unn. C [wt. %]	norm. C [wt. %]	Atom. C [at. %]	Error [%]
Carbon	K-series	23.59	23.70	83.46	3.5
Platinum	M-series	75.95	76.30	16.54	3.1
Total		99.53	100	100	

3.3 XRD results

To obtain more detailed information on the composition and crystal structure of the catalysts, XRD patterns (see Fig. 3. 7.) for all samples were obtained. Additionally, raw XC-72R was also studied to detect its peaks and differentiate it from the Pt crystallites.

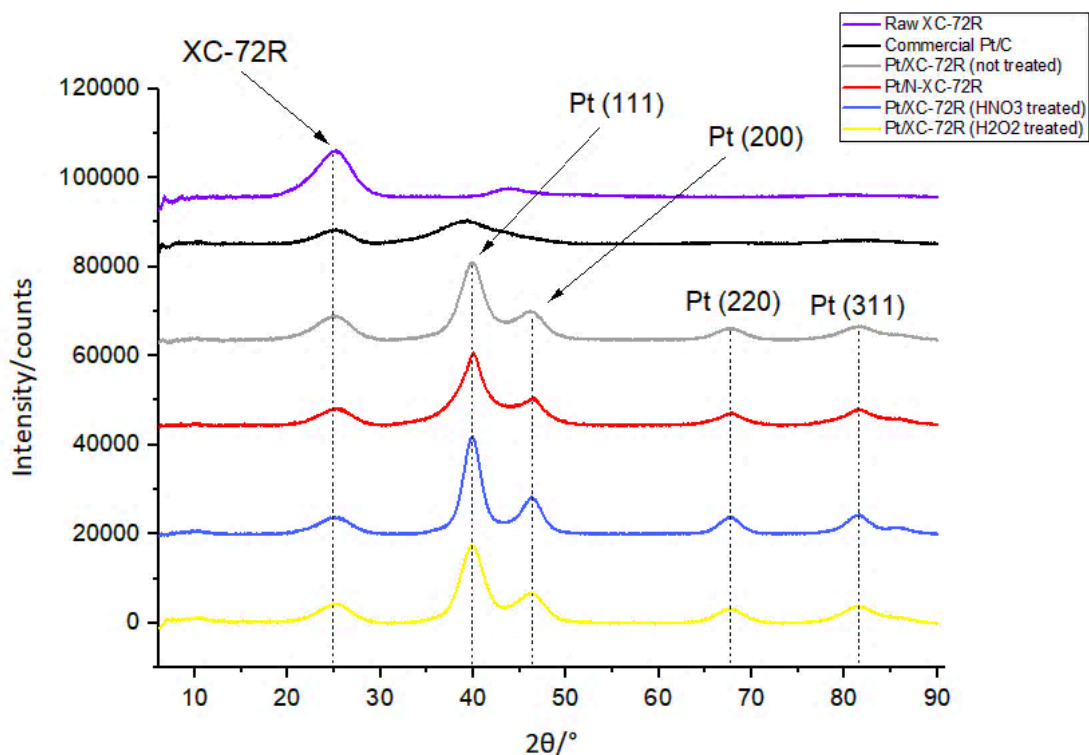


Fig. 3.7. X-ray diffraction (XRD) patterns for all samples

The peaks at Bragg angles of around 25° and 44° were attributed to the Vulcan XC-72R. For all synthesized catalyst samples, much flatter version (due to increased amorphous nature) of the peak at 25° was present indicating to XC-72R element in the sample. In terms of Pt, the peaks corresponding to the face-centered cubic (FCC) polycrystalline Pt (reflection planes of 111, 200, 220 and 311) were found which is in agreement with the JCPDS card number 00-4-0802 ($2\theta = 39.76^\circ, 46.24^\circ, 67.45^\circ, \text{ and } 81.28^\circ$ respectively) [53]. Furthermore, the crystallite size of all materials was calculated from the peak associated with the 111 reflection plane using the X'pert Highscore software and it is given in Table 3.4. below.

Table 3.4. Crystallite size for each sample (taken from the peak of 111 plane)

	Commercial Pt/C	Pt/XC (HNO ₃ treated)	Pt/XC (H ₂ O ₂ treated)	Pt/XC (non-treated)	Pt/N-XC (non-treated)
Cr. Size	1.5 (nm)	5.0	3.9	3.6	4.0

Calculated crystallite size for Pt/XC-72R (H₂O₂ treated) is similar to the results collected from the SEM measurement. At the same time, the size of the pre-treated samples is found to be higher than the non-treated sample suggesting an increase in particle size caused by the pre-treatment. If this is the case, HNO₃ treatment can be employed to produce bigger particles while H₂O₂ treatment may result in NPs with moderate particle size. It seems like N-doping of the non-treated XC also leads to crystallite size comparable to that of the H₂O₂ treated catalyst.

Furthermore, the obtained values show that commercial Pt/C has the lowest Pt crystallite size which can also be seen from its peak at around 40°. In addition, XRD pattern for the commercial sample did not show the smaller peak at 46° presumably due to missing 200 plane in the lattice and contribution of the XC-72R (which was not present in this case) at 44° while there were small-scale peaks at 67° and 81° associated with the 220 and 311 planes similar to rest of the samples.

3.4 Raman spectra

Raman spectroscopy was performed to analyze the structure of carbon black contained in each sample as demonstrated in Fig. 3.8.

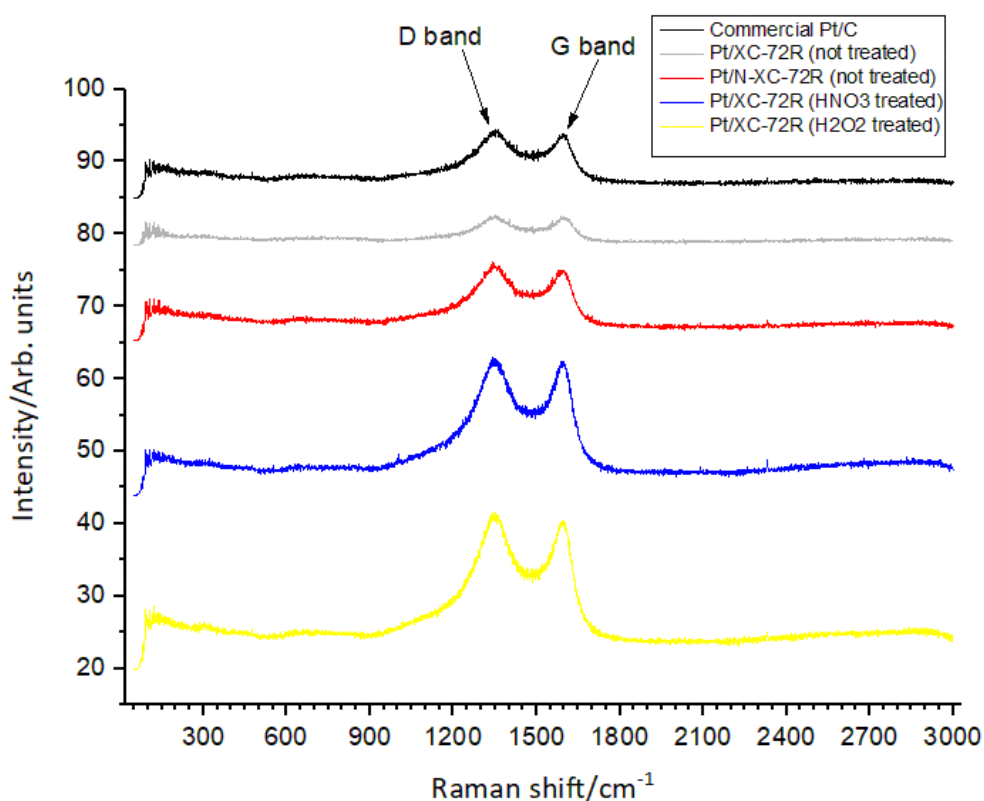


Fig. 3.8. Raman spectra for all samples (532 nm laser line)

Three main peaks (or bands) are often used to characterize Raman spectra of a given material: the so-called D-band, G-band, and 2D (or G') band. In this work, only first-order spectral range (1000 to 2000 cm^{-1}) is examined in which the corresponding D and G bands are shown in Fig. 3.8. It is possible to learn about the structural properties of carbon material by finding the Raman shift value for each peak. For example, the D-band is caused by a disorder in the edge of a microcrystalline structure while G-band is formed due to graphene presence [54].

As seen in the spectra, D and G-bands occur around 1345 and 1595 cm^{-1} in all of the samples. A considerable rise in the intensity level (for D-band) is observed in case of the pre-treated catalysts possibly due to increased disorder in the XC-72R structure caused by the heat treatment and N-doping of XC-72R in case of the N-doped catalyst. The commercial Pt/C catalyst has slightly smaller band peaks in comparison to the other materials corresponding to a more ordered structural form of carbon black contained in this catalyst.

To compare the crystallinity and disorder of the catalysts, analytically obtained peak values are given (see Table 3.5.) in the form of the Raman shifts related to both D and G-bands.

Table 3.5. D and G-band values for all samples obtained from Raman spectra

	Commercial Pt/C	Pt/XC (HNO ₃ treated)	Pt/XC (H ₂ O ₂ treated)	Pt/XC (non-treated)	Pt/N-XC (non-treated)
D band	1349.813 (cm ⁻¹)	1340.069	1342.611	1351.508	1340.493
G band	1594.693 (cm ⁻¹)	1590.033	1591.304	1598.930	1598.083
I_D^*	29.489	38.963	41.640	24.106	30.774
I_G^*	28.921	38.481	40.494	23.835	29.614
I_D/I_G	1.0196	1.0125	1.0283	1.0113	1.0391

* - in arbitrary units

The intensity ratio (I_D/I_G) of samples is often used to compare different materials based on their microstructure. For example, the ratio value for the H₂O₂ treated material is higher than the non-treated sample. This can be explained by decreased structural order and an increased number of defects in the composition of the Pt/XC-72R (H₂O₂ treated) catalyst. Increasing the number of defects on carbon black after treatment was a desirable property as this can be associated with a more porous structure with a higher number of sites for Pt deposition, thus better utilization, EASA value, and activity.

However, the crystal structure of the nitric acid-treated catalyst seems to be slightly more ordered like the non-treated material although its peak-intensity figures are comparable to that of the H₂O₂ treated sample. In case of the N-doped sample, the ratio number was maximum, and the intensity values were similar to the commercial Pt/C which can be translated more ordered structure with fewer defects in comparison to the pre-treated materials. Thus, the effect of N-doping on XC-72R seems to be minuscule in terms of its morphology.

4. CONCLUSIONS

This research focused on the influence of Vulcan XC-72R (carbon black) pre-treatment on the final properties of fuel cell catalyst materials with Pt nanoparticles. For this purpose, firstly catalyst samples with different treatment pathways (H_2O_2 and HNO_3 treatments) were synthesized via the polyol method using ethylene glycol. Next, in order to gain insight into the pre-treatment effect by comparison, the same type of synthesis was conducted for two additional samples to obtain catalysts with non-treated XC-72R and N-doped XC-72R (also non-treated). Finally, commercial Pt/C catalyst with 20% Pt loading was used as a benchmark for overall differentiation.

Different methods of material characterization were employed to study the samples. In case of the electrochemical characterization, EASA was calculated based on the H desorption charge associated with the peaks found in CV curves of all samples obtained at 10 mVs^{-1} . Calculations revealed that H_2O_2 treated material had the largest EASA surpassing the non-treated and commercial Pt/C catalyst while HNO_3 treatment resulted in much smaller EASA value. This suggests that H_2O_2 pre-treatment of XC-72R enhances the electrochemically active surface area of the final sample.

ORR activity of the catalysts was studied by comparing the LSV plateaus at a fixed rotation rate and onset potential values were acquired. It was identified that H_2O_2 treatment is linked to a considerable increase in the onset potential and excellent diffusion-limited current density value of $5.3 \text{ mA}\cdot\text{cm}^{-2}$ which is in the same magnitude with the corresponding theoretical value of $5.7 \text{ mA}\cdot\text{cm}^{-2}$ [47]. However, this was not observed in case of the Pt/XC-72R (HNO_3 treated) catalyst as its polarization curve was not much different in contrast to the non-treated material despite having a higher onset potential than the non-treated sample and being quite comparable to the plateau of commercial Pt/C. Furthermore, N-doping was observed to increase the ORR activity of XC-72R to a certain degree.

For a more detailed comparison, ORR polarization curves (at different rotation speeds) of Pt/XC-72R (H_2O_2 treated) and Pt/XC-72R (non-treated) catalysts were analyzed next to each other. Higher limiting current values and well-defined current density plateau of the pre-treated catalyst indicated to advanced oxygen reduction properties. At the same time, kinetic current density figures obtained from the KL plots showed that H_2O_2 treatment leads to about 10 times higher kinetic activity while HNO_3 treatment was associated with lower kinetic activity in contrast to the non-treated and commercial samples. The number of electrons involved in ORR was also calculated and it was

determined that all of the samples used the 4-electron pathway which is advantageous over the 2-electron pathway due to several reasons discussed in the relevant section.

Additionally, the electrochemical stability of the samples was investigated with accelerated stress testing of 500 potential cycles in which H₂O₂ treated catalyst exhibited superior stability while slightly higher current shifts at increasing voltages were observed for the rest of the materials.

SEM micrograph of Pt/XC-72R (H₂O₂ treated) catalyst confirmed the presence of Pt nanoparticles on carbon and NP size was estimated to be between 2.93-4.46 nm which is close to 4.4 nm that is considered to be an optimum size for enhanced mass activity in one study [52]. At the same time, the stoichiometric ratio of Pt and C was observed to agree with the synthesis protocol by analyzing the EDX spectra.

Concerning the XRD results, all synthesized samples (except commercial Pt/C) were associated with FCC polycrystalline Pt reflection planes with major peaks at 40° and 46° 2 θ . Crystallite size was calculated to be 3.9 nm for H₂O₂ treated material and 5.0 nm for the nitric acid-treated sample while the non-treated catalyst was in the range of 3.6 nm. This suggests that HNO₃ treatment of XC-72R results in catalysts with high particle size while H₂O₂ treatment leads to a minimal increase in particle size.

Lastly, in order to characterize the crystal structure and morphology of the XC-72R present in the samples, Raman spectra was obtained. Comparison of I_D/I_G ratio showed that Pt/XC-72R (H₂O₂ treated) catalyst material contains Vulcan carbon with less structural order and more defects in comparison to non-treated material which is desirable due to better Pt utilization connected with a higher number of defects. In relation to the nitric acid-treated sample, the crystal structure was assumed to be slightly more ordered although the peak intensities were analogous to that of the H₂O₂ treated catalyst. Despite having the maximum ratio value, N-doped catalyst's intensity levels were close to the commercial sample indicating a more ordered structure and fewer defects. This means that N-doping did not have much effect on the morphology of XC-72R.

To conclude, it is hypothesized that H₂O₂ pre-treatment of XC-72R results in a substantial increase in the catalytic activity of the final sample, and the next step can be further experimentation with this sample to find a balance between reducing the Pt loading and maintaining the desired ORR kinetics.

REFERENCES

- [1] Thompson, S.T., James, B.D., Huya-Kouadio, J.M., Houchins, C., DeSantis, D.A., Ahluwalia, R., Wilson, A.R., Kleen, G., Papageorgopoulos, D.: Direct hydrogen fuel cell electric vehicle cost analysis: system and high-volume manufacturing description, validation, and outlook. *J. Power Sources* 399, 304–313 (2018).
- [2] Breeze, P. (2017). *Fuel cells* (p. 4). London: Academic press.
- [3] Blomen, L., & Mugerwa, M. (1993). *Fuel Cell Systems* (p. 20). New York: Springer Science + Business Media.
- [4] Miranda, P. (2019). *Science and engineering of hydrogen-based energy technologies* (pp. 237-258). Elsevier.
<https://doi.org/10.1016/j.jpowsour.2018.07.100>
- [5] Shekhawat, Dushyant Spivey, J.J. Berry, David A.. (2011). *Fuel Cells - Technologies for Fuel Processing - 2.5.1 Direct Carbon Fuel Cell (DCFC)*. (pp. 20, 21). Elsevier. Retrieved from
<https://app.knovel.com/hotlink/pdf/id:kt00BIPZK4/fuel-cells-technologies/direct-carbon-fuel-cell>
- [6] TOYOTA MIRAI TECHNICAL SPECIFICATIONS. [Media.toyota.co.uk](https://media.toyota.co.uk). Retrieved 11 March 2020, from https://media.toyota.co.uk/wp-content/files_mf/1444919532151015MToyotaMiraiTechSpecFinal.pdf
- [7] Paul Breeze, Chapter 7 - Fuel Cells, Editor(s): Paul Breeze, *Power Generation Technologies (Third Edition)*, Newnes, 2019, Pages 145-171, ISBN 9780081026311, <https://doi.org/10.1016/B978-0-08-102631-1.00007-9>.
- [8] Holton, O. T., & Stevenson, J. W. (2013). The Role of Platinum in Proton Exchange Membrane Fuel Cells. *Platinum Metals Review*, 57(4), 260. doi: 10.1595/147106713x671222
- [9] Abdi, H., Rasouli Nezhad, R., & Salehimaleh, M. (2017). *Distributed Generation Systems* (pp. 231–232). Butterworth–Heinemann.
- [10] Emadi A., Ehsani M., Miller J.M. *Vehicular Electric Power Systems, Land, Sea, Air, and Space Vehicles*. Marcel Dekker; 2004.
- [11] Rashid M.H. *Modern Electric, Hybrid Electric, and Fuel Cell Vehicles Fundamentals, Theory, and Design*. second ed. Taylor and Francis; 2010.
- [12] Uzunoglu, M., & S.Alam, M. (2018). *Power electronics handbook* (4th ed., pp. 1091-1112). Butterworth-Heinemann.
- [13] Garce, J., & Moseley, P. T. (Eds.). (2014). *Electrochemical energy storage for renewable sources and grid balancing*. (page 147) Retrieved from <https://ebookcentral.proquest.com>

- [14] Arges, C., Ramani, V., & Pintauro, P. (2010). The Chalkboard: Anion Exchange Membrane Fuel Cells. *The Electrochemical Society Interface*, 19(2), 31-35. <https://doi.org/10.1149/2.f03102if>
- [15] Sudhakar, Y., Selvakumar, M., & Bhat, D. (2018). *Biopolymer electrolytes* (pp. 151-166). Elsevier.
- [16] Dincer, I., & Rosen, M. A. (2012). *Exergy : Energy, environment and sustainable development*. (page 365) Retrieved from <https://ebookcentral.proquest.com>
- [17] O'hayre, R., Cha, S., Colella, W., & Prinz, F. (2016). *Fuel Cell Fundamentals* (3rd ed., pp. 274, 275). WILEY.
- [18] Singhal, S., Kendall, K., & Kendall, M. (2015). *High-temperature solid oxide fuel cells: Fundamentals, design and applications*. (page 1) Retrieved from <https://ebookcentral.proquest.com>
- [19] Faizan, A. *Fuel Cell: Types, Working, Applications, Advantages & Disadvantages*. Retrieved 13 March 2020, from <https://electricalacademia.com/renewable-energy/fuel-cell-types-working-applications-advantages-disadvantages/>
- [20] Si, F., Zhang, Y., Yan, L., Zhu, J., Xiao, M., & Liu, C. et al. (2014). Electrochemical Oxygen Reduction Reaction. *Rotating Electrode Methods And Oxygen Reduction Electrocatalysts*, 133-170. <https://doi.org/10.1016/b978-0-444-63278-4.00004-5>
- [21] The Royal Society of Chemistry. (2016). *Oxygen Reduction Reaction*. Retrieved 16 April 2020, from <http://www.rsc.org/suppdata/c6/ra/c6ra23100d/c6ra23100d1.pdf>.
- [22] Khotseng, L. (2018). *Oxygen Reduction Reaction. Electrocatalysts For Fuel Cells And Hydrogen Evolution - Theory To Design*. <https://doi.org/10.5772/intechopen.79098>
- [23] Zhang, J., Xia, Z., & Dai, L. (2015). Carbon-based electrocatalysts for advanced energy conversion and storage. *Science Advances*, 1(7), e1500564. <https://doi.org/10.1126/sciadv.1500564>
- [24] H. A. Gasteiger and N. M. Marković, *Science*, 2009, 324, (5923), 48 [LINK http://dx.doi.org/10.1126/science.1172083](http://dx.doi.org/10.1126/science.1172083)
- [25] Ma, R., Lin, G., Zhou, Y., Liu, Q., Zhang, T., & Shan, G. et al. (2019). A review of oxygen reduction mechanisms for metal-free carbon-based electrocatalysts. *Npj Computational Materials*, 5(1). <https://doi.org/10.1038/s41524-019-0210-3>

- [26] Meier, J. C.; Galeano, C.; Katsounaros, I.; Witte, J.; Bongard, H. J.; Topalov, A. A.; Baldizzone, C.; Mezzavilla, S.; Schüth, F.; Mayrhofer, K. J. J. Beilstein J. Nanotechnol. 2014, 5, 44–67. doi:10.3762/bjnano.5.5
- [27] Nikiforov, Aleksey. (2011). New Construction and Catalyst Support Materials for Water Electrolysis at Elevated Temperatures. 10.13140/RG.2.1.3346.6087.
- [28] Kinoshita, K. (1988). Carbon: electrochemical and physicochemical properties.
- [29] Kim, M., Park, J., Kim, H., Song, S., & Lee, W. (2006). The preparation of Pt/C catalysts using various carbon materials for the cathode of PEMFC. Journal Of Power Sources, 163(1), 93-97. <https://doi.org/https://doi.org/10.1016/j.jpowsour.2006.05.057>
- [30] Li, Y., Liu, T., Yang, W., Zhu, Z., Zhai, Y., Gu, W., & Zhu, C. (2019). Multiscale porous Fe–N–C networks as highly efficient catalysts for the oxygen reduction reaction. Nanoscale, 11(41), 19506-19511. <https://doi.org/10.1039/c9nr05726a>
- [31] Kumar, S., Hidyatai, N., Herrero, J., Irusta, S., & Scott, K. (2011). Efficient tuning of the Pt nano-particle mono-dispersion on Vulcan XC-72R by selective pre-treatment and electrochemical evaluation of hydrogen oxidation and oxygen reduction reactions. International Journal Of Hydrogen Energy, 36(9), 5453-5465. <https://doi.org/10.1016/j.ijhydene.2011.01.124>
- [32] Holade, Y., Sahin, N., Servat, K., Napporn, T., & Kokoh, K. (2015). Recent Advances in Carbon Supported Metal Nanoparticles Preparation for Oxygen Reduction Reaction in Low Temperature Fuel Cells. Catalysts, 5(1), 310-348. <https://doi.org/10.3390/catal5010310>
- [33] Debe, M. Electrocatalyst approaches and challenges for automotive fuel cells. Nature 486, 43–51 (2012). <https://doi.org/10.1038/nature11115>
- [34] Lemus, J., Bedia, J., Calvo, L., Simakova, I., Murzin, D., & Etzold, B. et al. (2016). Improved synthesis and hydrothermal stability of Pt/C catalysts based on size-controlled nanoparticles. Catalysis Science & Technology, 6(13), 5196-5206. <https://doi.org/10.1039/c6cy00403b>
- [35] Alegre, C., Gálvez, M., Moliner, R., & Lázaro, M. (2015). Influence of the Synthesis Method for Pt Catalysts Supported on Highly Mesoporous Carbon Xerogel and Vulcan Carbon Black on the Electro-Oxidation of Methanol. Catalysts, 5(1), 392-405. <https://doi.org/10.3390/catal5010392>
- [36] RAO, C., & TRIVEDI, D. (2005). Chemical and electrochemical depositions of platinum group metals and their applications. Coordination Chemistry Reviews, 249(5-6), 613-631. <https://doi.org/10.1016/j.ccr.2004.08.015>

- [37] Liu, H., Song, C., Zhang, L., Zhang, J., Wang, H., & Wilkinson, D. (2006). A review of anode catalysis in the direct methanol fuel cell. *Journal Of Power Sources*, 155(2), 95-110. <https://doi.org/10.1016/j.jpowsour.2006.01.030>
- [38] Martín, A., Chaparro, A., Gallardo, B., Folgado, M., & Daza, L. (2009). Characterization and single cell testing of Pt/C electrodes prepared by electrodeposition. *Journal Of Power Sources*, 192(1), 14-20. <https://doi.org/10.1016/j.jpowsour.2008.10.104>
- [39] FIEVET, F., LAGIER, J., BLIN, B., BEAUDOIN, B., & FIGLARZ, M. (1989). Homogeneous and heterogeneous nucleations in the polyol process for the preparation of micron and submicron size metal particles. *Solid State Ionics*, 32-33, 198-205. doi: 10.1016/0167-2738(89)90222-1
- [40] Bensebaa, F. (2013). Wet Production Methods. *Interface Science And Technology*, 85-146. doi: 10.1016/b978-0-12-369550-5.00002-1
- [41] Qi, J., Jiang, L., Jing, M., Tang, Q., & Sun, G. (2011). Preparation of Pt/C via a polyol process – Investigation on carbon support adding sequence. *International Journal Of Hydrogen Energy*, 36(17), 10490-10501. <https://doi.org/10.1016/j.ijhydene.2011.06.022>
- [42] Rao, B., Mukherjee, D., & Reddy, B. (2017). Novel approaches for preparation of nanoparticles. *Nanostructures For Novel Therapy*, 1-36. doi: 10.1016/b978-0-323-46142-9.00001-3
- [43] Ratso, S., Kruusenberg, I., Käärik, M., Kook, M., Saar, R., & Pärs, M. et al. (2020). Highly efficient nitrogen-doped carbide-derived carbon materials for oxygen reduction reaction in alkaline media.
- [44] Lee, S., Pyun, S., Lee, S., & Kang, S. (2008). Fundamentals of Rotating Disc and Ring-Disc Electrode Techniques and their Applications to Study of the Oxygen Reduction Mechanism at Pt/C Electrode for Fuel Cells. *Israel Journal Of Chemistry*, 48(3-4), 215-228. <https://doi.org/10.1560/ijc.48.3-4.215>
- [45] Chou, H., Hwang, B., & Sun, C. (2013). Catalysis in Fuel Cells and Hydrogen Production. *New And Future Developments In Catalysis*, 217-270. <https://doi.org/10.1016/b978-0-444-53880-2.00014-4>
- [46] Habibi, B., & Ghaderi, S. (2016). Ethanol electrooxidation on the Co@Pt core-shell nanoparticles modified carbon-ceramic electrode in acidic and alkaline media. *Dx.doi.org*. Retrieved 3 May 2020, from <http://dx.doi.org/10.22104/ijhfc.2016.314>.
- [47] Garsany, Y., Baturina, O., Swider-Lyons, K., & Kocha, S. (2010). Experimental Methods for Quantifying the Activity of Platinum Electrocatalysts for the Oxygen Reduction Reaction. *Analytical Chemistry*, 82(15), 6321-6328. <https://doi.org/10.1021/ac100306c>

- [48] Zhao, Y., Chu, Y., Ju, X., Zhao, J., Kong, L., & Zhang, Y. (2018). Carbon-Supported Copper-Based Nitrogen-Containing Supramolecule as an Efficient Oxygen Reduction Reaction Catalyst in Neutral Medium.
- [49] Liu, R., Wu, D., Feng, X., & Müllen, K. (2010). Nitrogen-Doped Ordered Mesoporous Graphitic Arrays with High Electrocatalytic Activity for Oxygen Reduction. *Angewandte Chemie International Edition*, 49(14), 2565-2569. <https://doi.org/10.1002/anie.200907289>
- [50] Palomar-Pardavé, M. (2009). Electrochemical applications to biology, nanotechnology, and environmental engineering and materials (p. 272). The Electrochemical Society.
- [51] Zhang, W., Shaikh, A., Tsui, E., & Swager, T. (2009). Cobalt Porphyrin Functionalized Carbon Nanotubes for Oxygen Reduction. *Chemistry Of Materials*, 21(14), 3234-3241. <https://doi.org/10.1021/cm900747t>
- [52] Xu, Z., Zhang, H., Zhong, H., Lu, Q., Wang, Y., & Su, D. (2012). Effect of particle size on the activity and durability of the Pt/C electrocatalyst for proton exchange membrane fuel cells. *Applied Catalysis B: Environmental*, 111-112, 264-270. <https://doi.org/10.1016/j.apcatb.2011.10.007>
- [53] Videla, A., Osmieri, L., Esfahani, R., Zeng, J., Francia, C., & Specchia, S. (2015). The Use of C-MnO₂ as Hybrid Precursor Support for a Pt/C-Mn_xO_{1+x} Catalyst with Enhanced Activity for the Methanol Oxidation Reaction (MOR). *Catalysts*, 5(3), 1399-1416. <https://doi.org/10.3390/catal5031399>
- [54] Characterizing Carbon Nanomaterials with a Raman Analyzer. AZoM.com. (2018). Retrieved 19 May 2020, from <https://www.azom.com/article.aspx?ArticleID=14826>.